USGS
science for a changing world

EPA

Prepared for the U.S. Environmental Protection Agency

Geophysical Logging Data from the Mills Gap Road area near Asheville, North Carolina

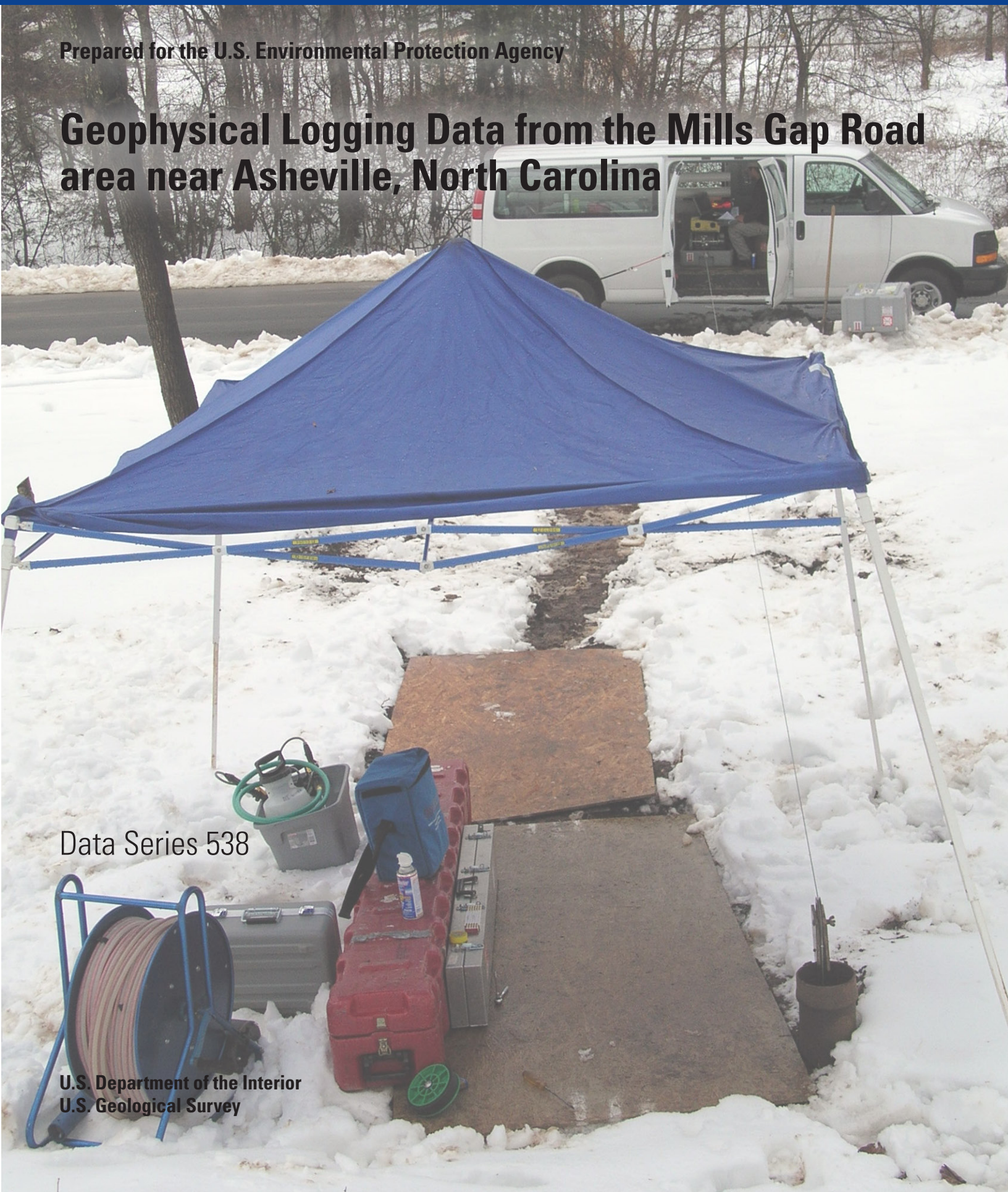

Data Series 538

U.S. Department of the Interior
U.S. Geological Survey

Cover. Heat-pulse flowmeter logging at well AW-7 near Asheville, North Carolina, February 2010 *(photograph by John Mazurek, USGS)*.

Geophysical Logging Data from the Mills Gap Road area near Asheville, North Carolina

By Melinda J. Chapman and Brad A. Huffman

Prepared for the U.S. Environmental Protection Agency Region 4 Superfund Section

Data Series 538

U.S. Department of the Interior
U.S. Geological Survey

U.S. Department of the Interior
KEN SALAZAR, Secretary

U.S. Geological Survey
Marcia K. McNutt, Director

U.S. Geological Survey, Reston, Virginia: 2011

Suggested citation:
Chapman, M.J., and Huffman, B.A., 2011, Geophysical logging data from the Mills Gap Road area near Asheville, North Carolina: U.S. Geological Survey Data Series 538, 49 p. + attachment.

(Available only online at http://pubs.usgs.gov/ds/538/)

Contents

Figures

Tables

Appendixes

Attachment 1

Conversion Factors

Inch/Pound to SI

Multiply	By	To obtain
inch (in.)	2.54	centimeter (cm)
inch (in.)	25.4	millimeter (mm)
foot (ft)	0.3048	meter (m)
mile (mi)	1.609	kilometer (km)
gallon per minute	0.06309	liter per second (L/s)

Temperature is given in degrees Fahrenheit (°F), which can be converted to degrees Celsius (°C) as follows:

$$°C = (°F - 32) / 1.8$$

Specific conductance is given in microsiemens per centimeter at 25 degrees Celsius (µS/cm).

Vertical coordinate information is referenced to the North American Vertical Datum of 1988 (NAVD 88).

Horizontal coordinate information is referenced to the North American Datum of 1983 (NAD 83).

Altitude, as used in this report, refers to distance above the vertical datum.

Geophysical Logging Data from the Mills Gap Road area near Asheville, North Carolina

By Melinda J. Chapman and Brad A. Huffman

Background and Description of Methods

In September 2009, the U.S. Geological Survey (USGS) was requested to assist the U.S. Environmental Protection Agency (EPA) Region 4 Superfund Section in the development of a conceptual groundwater flow model in the area of the Mills Gap Road contaminant investigation near Asheville, North Carolina (Site ID A4P5) through an Interagency Grant and work authorization IAD DW number 14946085. The USGS approach included the application of established and state-of-the-science borehole geophysical tools and methods used to delineate and characterize fracture zones in the regolith-fractured bedrock groundwater system. Borehole geophysical logs were collected in eight wells in the Mills Gap Road project area from January through June 2010. These subsurface data were compared to local surface geologic mapping data collected by the North Carolina Geological Survey (NCGS) from January through May 2010.

Borehole geophysical logs and surface geologic mapping methods were used to characterize both subsurface and surface features in the fractured bedrock and overlying regolith. As in most areas of the Piedmont and Blue Ridge Physiographic Provinces in the southeastern United States, the groundwater system in the metamorphic and igneous rocks is complex and directly related to multiple periods of structural deformation, metamorphism, and igneous intrusion. The groundwater system in the Blue Ridge Physiographic Province consists of two components—a shallow regolith component that may include soil, saprolite, debris flow material, colluvium, and alluvium, and a deeper fractured-bedrock component (Chapman and others, 2005). Where present in the Blue Ridge Physiographic Province, the regolith is the primary storage reservoir and is the source of recharge to the bedrock fractures (Heath, 1980, 1983, 1984, 1994; Heath and Jennings, 1995). The bedrock has little primary porosity except where secondary openings are present in the form of fractures and other discontinuities. These secondary openings are the primary source of permeability. The bedrock is described by the NCGS as composed of the regional Ashe Metamorphic Suite-Tallulah Falls Formation, a metamorphosed and deformed package of sediments of Late Proterozoic to Middle Ordovician age that are interlayered with minor mafic intrusives and volcanics. Lithologies consist of metagraywacke, schistose metagraywacke, garnet mica schist, amphibolite, quartz and quartz-tourmaline veins, and lesser zones of fault breccia and gouge (Wooten and others, 2010). The observed regolith component of the groundwater system in the study area is described by Wooten and others (2010) as consisting of transported colluvial and alluvial deposits and residual soil formed from the in-place weathering of bedrock. MACTEC, Inc. (2009) reported following a Phase 1 Remedial Investigation of the Mills Gap Road site that the zone of overburden (regolith), determined from boreholes at the CTS Corporation of Asheville site, ranges in thickness from 28 to 81 feet (ft) below land surface (bls). This site is the location of a former electroplating facility, hereafter referred to in this report as the CTS site.

Dominant structural features and discontinuities described in the report by Wooten and others (2010) describe regional bedrock foliation and compositional layering as principally striking to the north-northeast and northeast and, to a lesser extent, to the north-northwest, except in the vicinity of the Mills Gap Fault Zone (MGFZ). Foliation, compositional layering and a younger mylonitic foliation are incrementally realigned near the MGFZ from a regional northeast-southwest strike trend to a west-northwest–east-southeast trend that is subparallel to the fault zone.

Three surface joint sets are described in the report by Wooten and others (2010). One joint set is associated with the MGFZ and is grouped into the following strike azimuths: 115 degrees (°) and 295° parallel to the fault and 85° and 265° conjugate to the fault trend. A second joint set includes strike azimuths of 25° and 205° that are subparallel to the predominant northeast-southwest bedrock layering and regional foliation, as well as north-northeast trending outcrop-scale faults, and north-northeast-trending secondary quartz and tourmaline veins. The third joint set includes strike azimuths of 145° and 325°, northwest-southeast striking that may also include some joints associated with the MGFZ, and 175° and 355°, regional north-south striking joints that may include some joints subparallel to the predominant north-south striking foliation (Wooten and others, 2010).

From January through June 2010, borehole geophysical logs were collected from a total of eight open-borehole

bedrock wells in the Mills Gap Road investigation area in the vicinity of the CTS site (table 1; fig. 1). Six of the wells (AW-4, AW-5, AW-7, ERT-7, Oaks-2, and ERT-6) were located in the Oaks subdivision, approximately 0.5 mile (mi) northeast of the site; one well (CHR) was located on Chapel Hill Church Road, approximately 0.37 mi northeast of the site; and one well (Well 1) was located on Concord Road, approximately 0.25 mi southeast of the site. Well depths ranged from 152 to 705 ft bls (table 1). From the compilation of casing depths listed in table 1, the regolith thickness inferred ranges from 6.5 to 70 ft. Additionally, fracture orientations from acoustic televiewer (ATV) image logs were available for four wells on the CTS site (fig. 1; table 1). Logs collected from each of the eight wells included caliper, electrical resistivity, natural gamma, fluid temperature and resistivity, heat-pulse flowmeter (both ambient and stressed), and optical televiewer (OTV). ATV logs were run in two wells as part of the quality-assurance procedures for the OTV tool. Field notes from geophysical logging activities are included in Attachment 1. Fracture zones were delineated at depth in each well by using all of these borehole logs. The fracture delineations were then used to guide the selection of downhole straddle-packer sampling by the EPA Environmental Response Team (ERT) and their contractors. Fracture orientations were determined from OTV images. The fracture orientation data were compared and used along with surface geologic mapping data to build a conceptual model of groundwater flow in the study area. Results of the NCGS surface geologic mapping study are described in Wooten and others (2010).

A Note about Conventions Used to Record Orientation Data

Bedrock discontinuities measured and recorded for this study are planar features. Dip directions were recorded using the convention that horizontal planes are recorded as having 0 degree dips, with values increasing for more steeply dipping features toward 90° for vertical features. For planar features, strike is defined as the compass orientation of the horizontal line lying within that plane. Strike azimuths of 0 to 360° were recorded using the familiar convention in which 0 and 360° correspond to map true north, 90° corresponds to east, 180° corresponds to south, etc. Because all lines extend in two directions, bedrock discontinuities were measured and recorded using the right-hand rule convention (strike azimuth is measured with the dip inclined toward the right). Two planar features assigned strikes that are parallel (for example, 45° and 225°) differ in that one feature dips to the southeast and the other to the northwest, respectively.

Table 1. U.S. Geological Survey well-logging and available construction data for wells at the CTS site.

[USGS, U.S. Geological Survey; NAD 83, North American Datum of 1983; NAVD 88, North American Vertical Datum of 1988; —, information not available; na, not applicable]

Well number	USGS site number	USGS county number	Latitude (decimal degrees) (NAD 83)	Longitude (decimal degrees) (NAD 83)	Land surface elevation (above NAVD 88)	Casing depth (feet below land surface)	Total depth (feet below land surface)	Reported well yield (gallons per minute)
Well 1	352932082300401	BU-111	35.49239	–82.50133	2,329.19	70	300	—
CHR	352948082300101	BU-110	35.496790	–82.50027	2,415.63	31	505	60
AW-4	352958082295301	BU-109	35.499480	–82.49799	2,399.75	62	707	2
AW-5	352958082295101	BU-106	35.499360	–82.49744	2,379.06	36	575	10
AW-7	352959082294901	BU-105	35.499940	–82.49689	2,330.26	17	576	20
ERT-7	352957082294801	BU-104	35.499120	–82.49677	2,313.47	7.5	152	—
Oaks-2	352957082295501	BU-108	35.499100	–82.49873	2,365.53	24	600	—
ERT-6	352956082295701	BU-107	35.498920	–82.49911	2,350.96	6.5	167	—
CTS-MW-1B	na	na	35.49179	–82.50682	2,439.39	68	146	—
CTS-MW-4B	na	na	35.49307	–82.50728	2,413.13	75	98	—
CTS-MW-9B	na	na	35.49357	–82.50434	2,415.11	63	80	—
CTS-MW-11B	na	na	35.49228	–82.50389	2,349.19	52	191	—

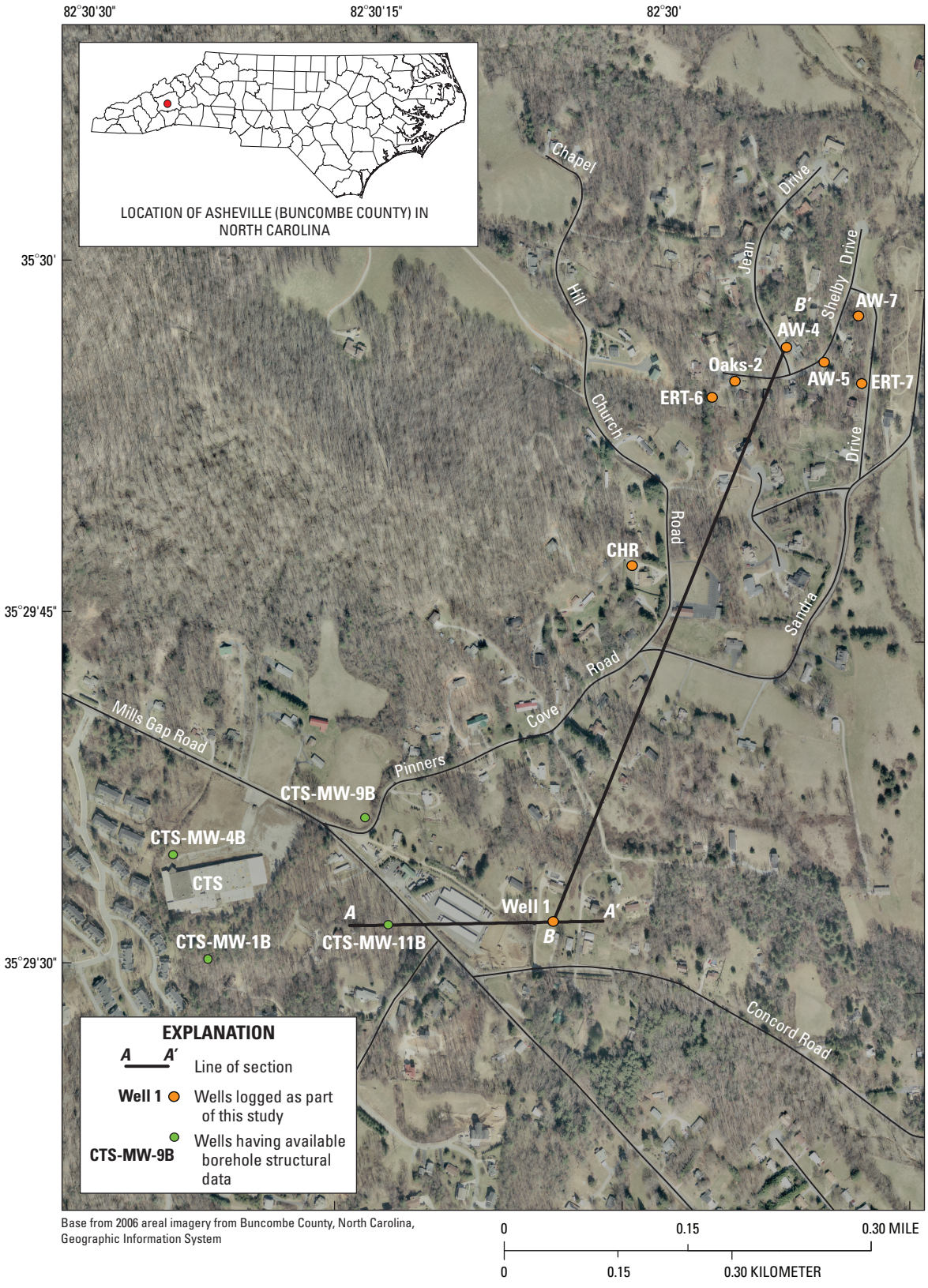

Figure 1. Distribution of wells having available borehole structural data and cross-section lines in the study area near Asheville, North Carolina.

A Note about Sampling Biases Inherent in the Borehole Surveys and the Surface Outcrop Measurements

Cursory inspection of the structural data tables and diagrams in this report and in the Wooten and others (2010) report show differences in their relative abundances of planar features counted within the various general orientation classes. This does not mean that the two sets of data are inconsistent with each other but rather that the two datasets are more useful when used together. Vertical boreholes are statistically less likely to intersect steeply dipping planar features than more flat-lying features, whereas surface outcrops provide a relatively better sample of more steeply dipping features. With the exception of the rare steep cliff face or high road cut, outcrops provide relatively less opportunity to count and measure flat-lying features.

Another difference is in the way features were tabulated in the two studies. When interpreting features in borehole images, hydrogeologists measure and count individual features. During surface mapping, geologists assign measurements to sets of features with similar orientation. For any given map station, which may represent an entire outcrop or group of outcrops, one recorded measurement could represent a group of 1 or 10 or 100 parallel similar joints or foliations.

Brittle features tabulated for outcrops throughout the entire NCGS study area are dominated by west-northwest and east-southeast trending features. NCGS geologists visited a relatively large number of outcrops located within the MGFZ, partly because the steep terrain in the MGFZ affords numerous outcrops for study and partly because the NCGS were motivated to gain all available information about the structure, which crosses the CTS site. As a result it is useful to consider the statistics for brittle outcrop data in separate sets—one set for the data collected from the MGFZ and another set for the data collected outside the MGFZ.

Borehole Geophysical Logging and Imaging

Data analyses from the collected downhole geophysical logs and images from the eight wells include the delineation of fracture zones and vertical borehole flow that were used for later packer sampling conducted by the EPA's ERT and their contractors during March through May 2010. Appendix 1 contains borehole diagrams showing geophysical logs and measured flow for each well logged. Most wells had measurable inflow at depth and outflow at shallow fracture zones (fig. 2; Appendix 1). Well 1 had measured upflow throughout the entire borehole and was flowing at land surface (see Field Notes, Attachment 1).

Further characterization of subsurface bedrock structures from the OTV images consisted of measuring the orientations of downhole bedrock foliation, lithologic contacts, and fractures. Orientations of subsurface foliation, lithologic contacts, and fractures were determined by using WellCad® software (from the OTV image; aLt, 2010). Fractures were characterized as either primary (open; indicated by blue tadpole symbols in Appendix 1) or secondary (partially open or weathered; indicated by red tadpole symbols in Appendix 1). Orientations interpreted from the OTV image logs were adjusted for a local magnetic declination of 6° west and for measured borehole deviation. Subsurface geologic features were imported into Rockworks™ software (Rockware, Inc., 2010) for statistical analyses using rose diagrams and three-dimensional display of fracture planes at depth.

More than 8,700 subsurface structural measurements (orientations) were interpreted from OTV images collected from the eight wells logged in the Mills Gap Road project area. Additionally, fracture orientation data were available from interpretations of ATV image logs from four wells at the CTS site (Marv Gobles, CTS Corporation, written commun., January 2010). Figure 3 presents strike orientations for all structures measured in the eight wells logged by the USGS and available fracture orientations from the four CTS wells. Figure 4 presents an expanded view of orientations measured in the six wells in the Oaks subdivision area. Dominant orientations of structures logged in the eight individual wells logged by the USGS are listed in table 2, with the most common strike orientations being 10–20° and 20–30°. The dominant orientation of the combined borehole structures in the 12 wells trends to the northeast, striking from 0 to 30° (fig. 5), which parallels the north-northeast-trending regional bedrock foliation trend mapped by the NCGS throughout much of the Mills Gap Road project area except in the MGFZ, which has a west-northwest–east-southeast trend (Wooten and others, 2010). Most fractures observed in the downhole OTV images were parallel to foliation, or "foliation-parting" fractures (Williams and others, 2005). With the dominant subsurface features measured being primarily confined to a 0–30° strike orientation, there is potential for anisotropy (permeability increases in a particular direction) in the groundwater flow in this direction that could affect contaminant migration within the groundwater system in this area.

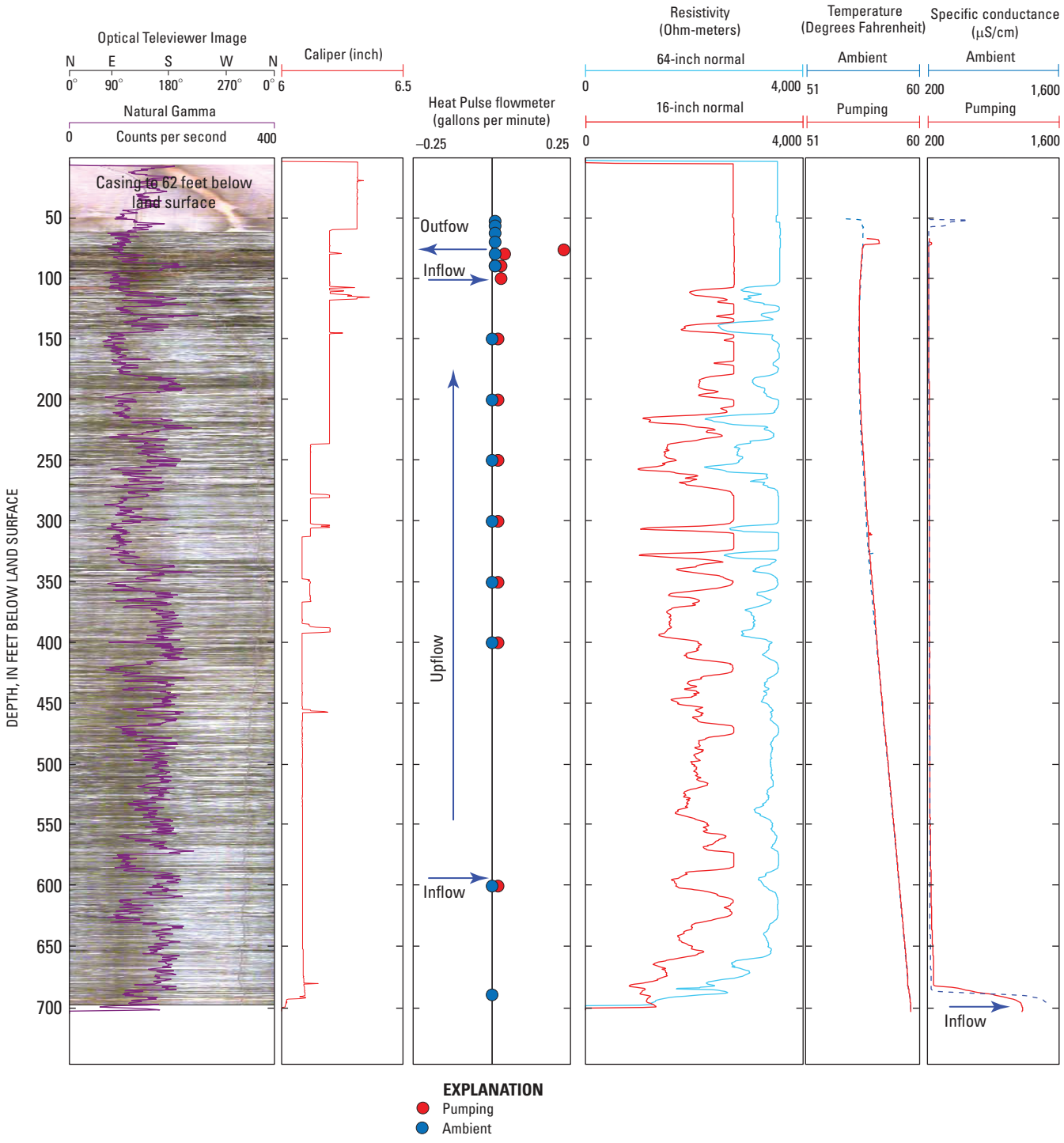

Figure 2. AW-4 borehole geophysical logs showing fracture zones and vertical flow within the well.

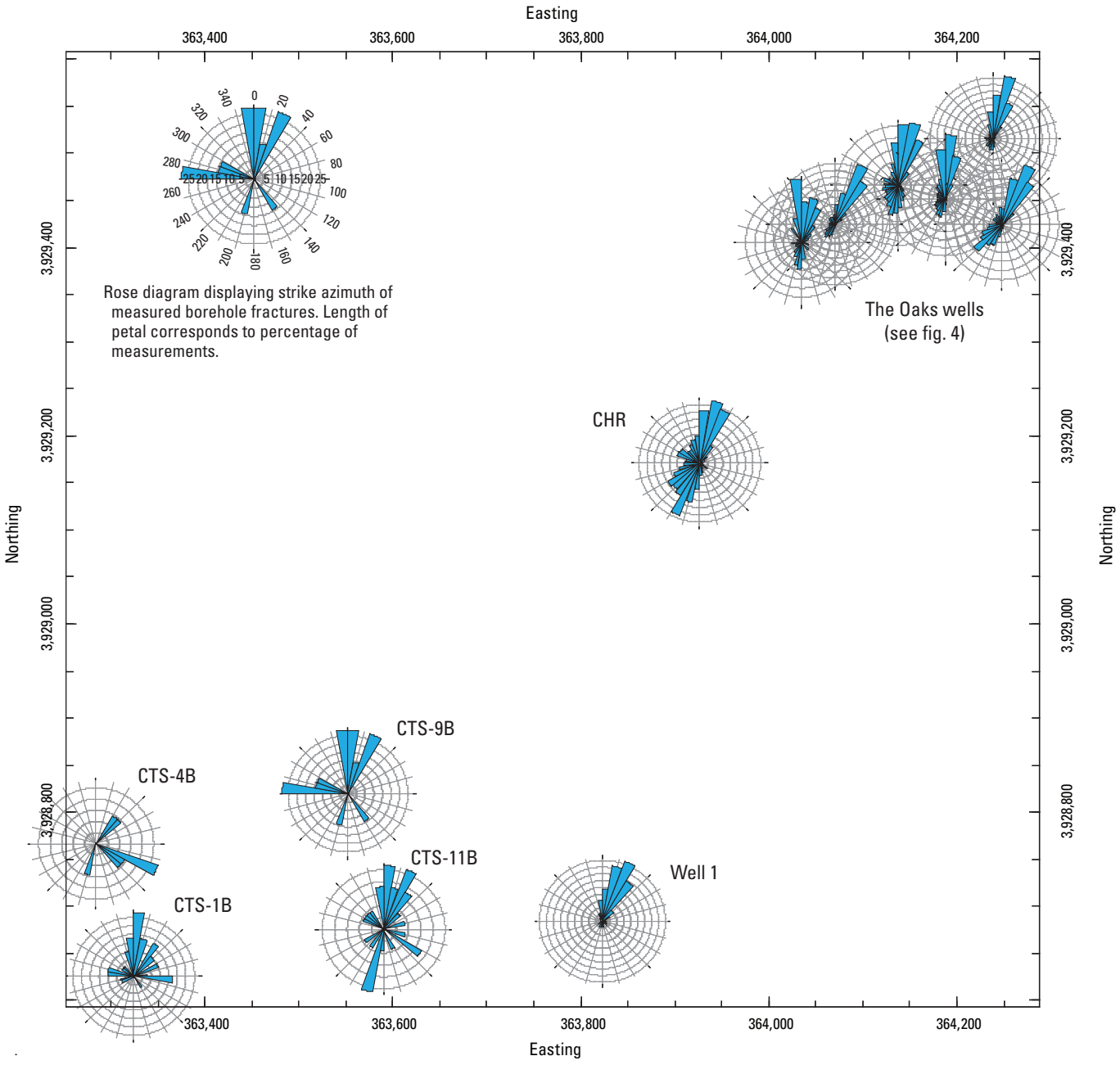

Figure 3. Rose diagrams showing strike orientations of all structures measured in Well 1, well CHR, and the Oaks wells, and fracture orientations reported in four CTS wells.

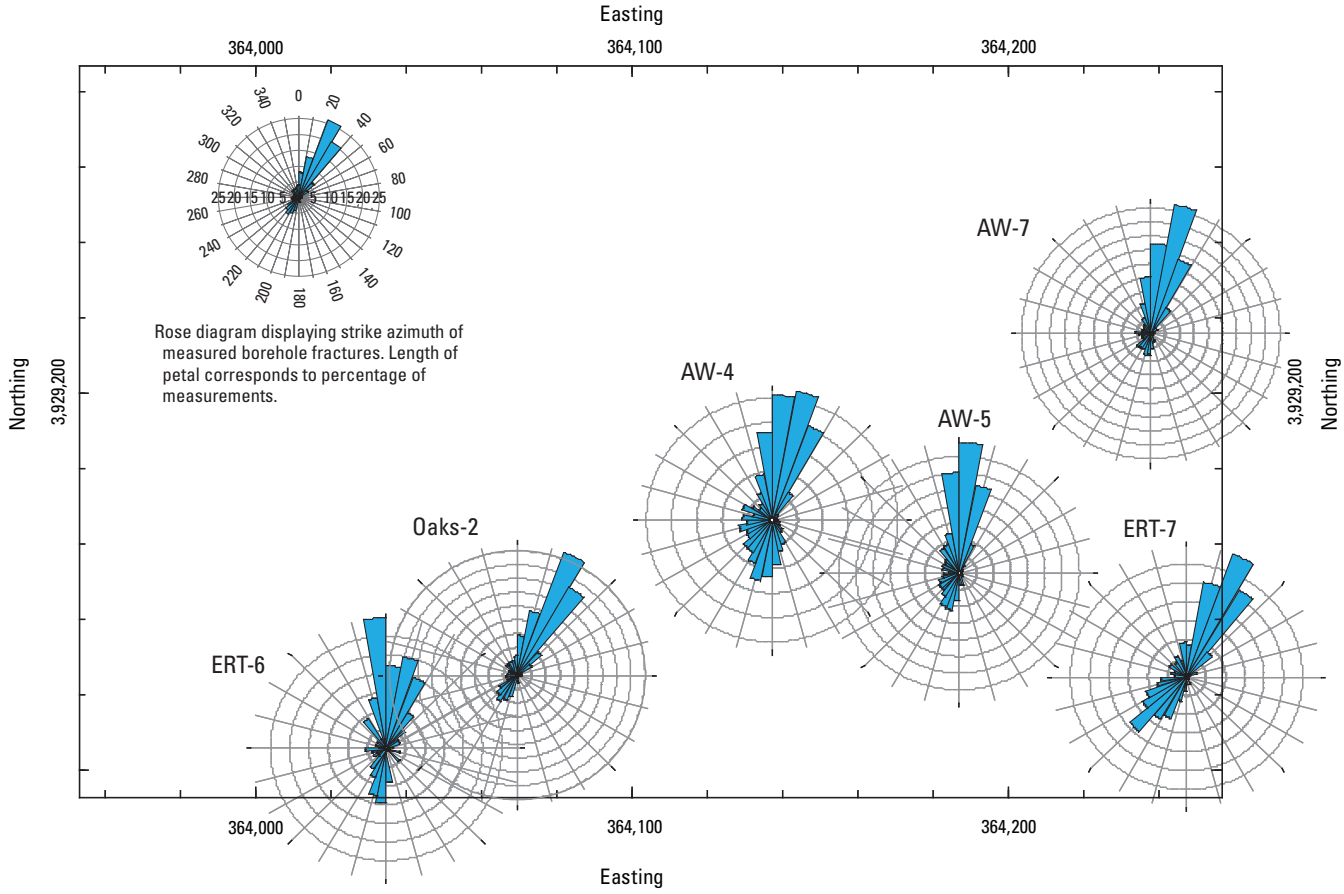

Figure 4. Rose diagrams showing strike orientations of all structures measured in the Oaks wells.

Table 2. Listing of dominant fracture strike azimuth for packer depth intervals.

Well number	All structures strike azimuth per 10-degree (°) bin (see rose diagrams in Appendix 3)			
	0–10°	10–20°	20–30°	350–360°
Well 1			X	
CHR		X		
AW-4		X		
AW-5	X			
AW-7		X		
ERT-7			X	
Oaks-2			X	
ERT-6				X

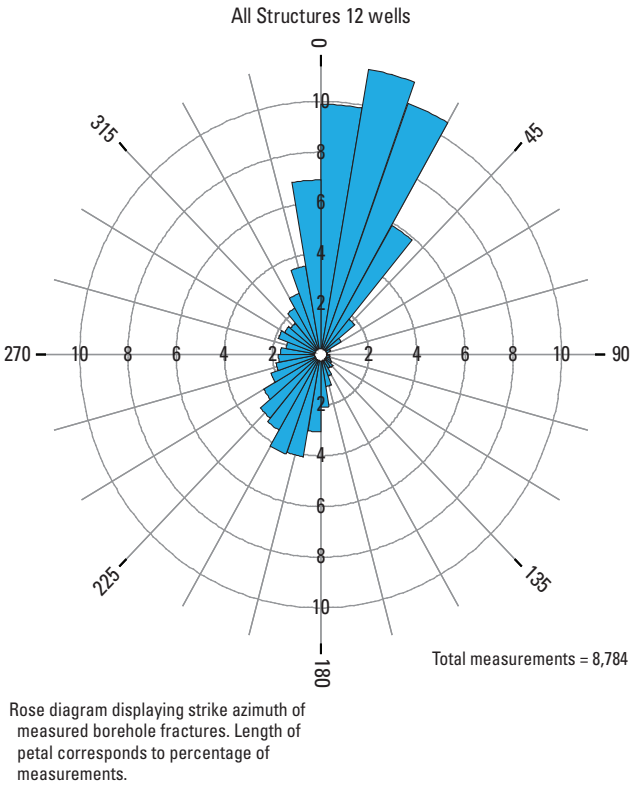

Figure 5. Rose diagram showing combined strike orientations of all structures measured in the eight wells logged as part of this study and the four CTS wells.

Subsurface Foliation

Subsurface foliation from the eight wells logged by the USGS were delineated (green tadpoles, Appendix 1) primarily striking 10–20° and 190–200° (table 3), with opposing dip directions. Most borehole foliation populations indicated a bimodal dip azimuth grouping (Appendix 2) with a secondary, parallel foliation set having strikes of about 200° (see A Note about Conventions Used to Record Orientation Data above**)** and dipping in the opposite direction, to the northwest. The bimodal distribution of subsurface foliation dip direction may be the result of local-scale folding, where fold axes have hinges with similar trends as foliation (Wooten and others, 2010; see borehole example in fig. 6). The 10–20° orientation is more representative of the surface geologic mapping data. The 190–200° orientation may be a factor of the sampling method in a vertical borehole (well). This apparent discrepancy is described in the section above; see A Note about Sampling Biases Inherent to the Borehole Surveys and the Surface Outcrop Measurements). Borehole logs collected in vertical wells favor the occurrence of encountering low-angle features, such as foliation, in this area or simply a fact of sampling a greater depth of section (as much as 700 ft bls in well AW-4).

Table 3. Listing of dominant foliation strike azimuth in the wells.

[Color designations correlate strike azimuth groups having the same bidirectional strike direction with opposite dip directions. >, greater than; X, primary; Y, secondary]

Well number	Fracture strike azimuth per 10-degree (°) bin (see rose diagrams in Appendix 3)									
	0–10°	>10–20°	>20–30°	>170–180°	>180–190°	>190–200°	>200–210°	>210–220°	>220–230°	>350–360°
Well 1		X		Y		Y				
CHR		X					Y			
AW-4	X	X			Y					
AW-5	X					Y	Y			
AW-7		X				Y				
ERT-7			X						Y	
Oaks-2			X					Y		
ERT-6						Y				X

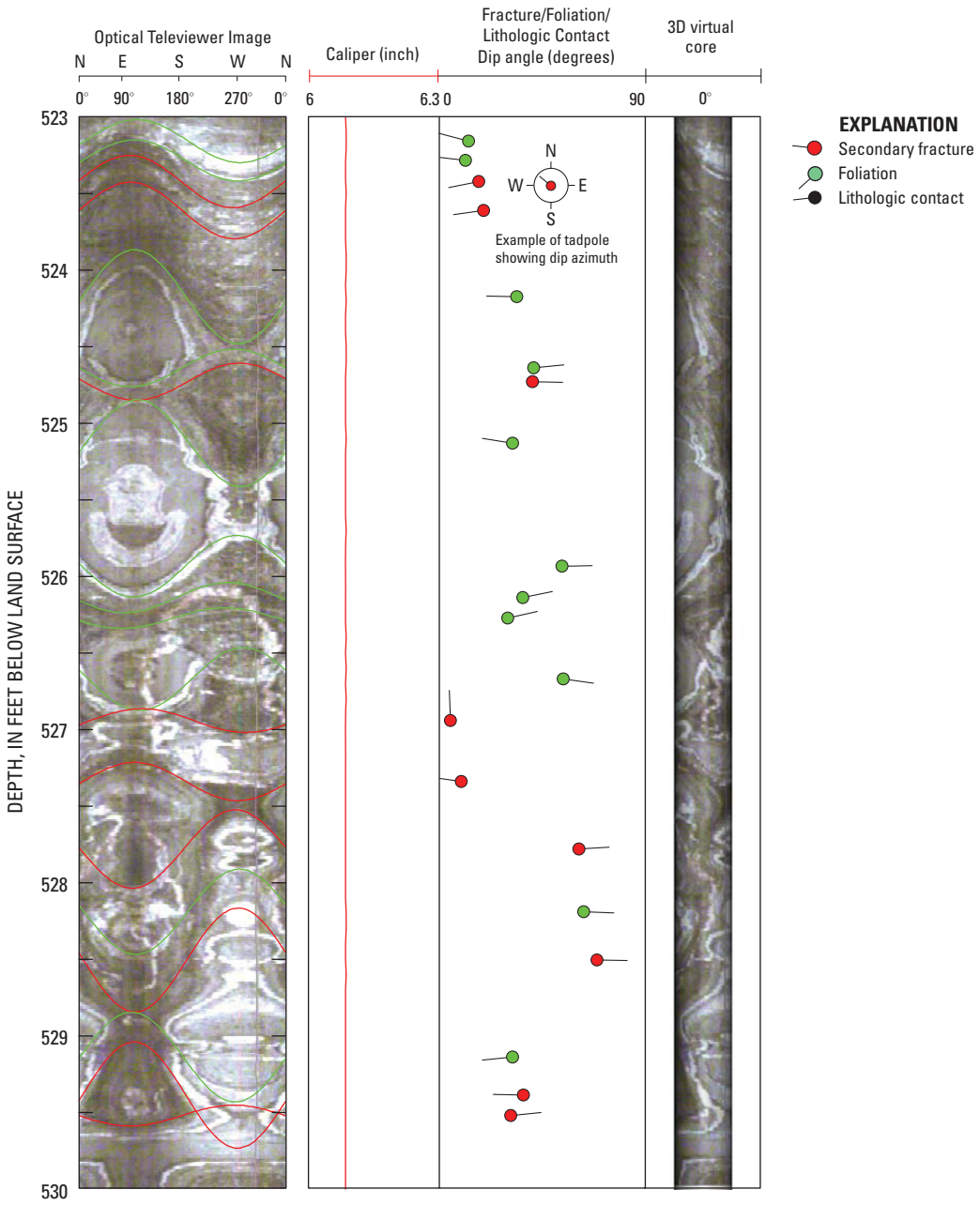

Figure 6. Example of folding and reversal of foliation dip direction observed in well AW-4.

These borehole foliation measurements are consistent with the style and orientation of foliations described by the NCGS based on their mapping of surface exposures in the study area:

> *Bedrock foliation and compositional layering strike principally to the NNE and NE, and to a lesser extent, to the NNW, except in the vicinity of the Mills Gap Fault Zone (MGFZ).....foliations, compositional layering, and a younger mylonitic foliation indicate these fabrics are incrementally realigned near the MGFZ from a regional NE-SW strike trend to that of a WNWESE trend subparallel to the MGFZ. Outcrop-scale ductile folds deform bedrock foliation. Observed ductile folds have hinges with similar trends as foliation and are gently inclined to recumbent with northwest vergence.*
>
> *Overall, bedrock foliation generally dips toward the SE except where locally deformed by folding, and realignment in proximity to the MGFZ* (Wooten and others, 2010).

The bimodal nature of foliation dips measured in the subsurface wells, most of which are located outside of the MGFZ, can be explained by their position in the noses of the type of folds described above. That most measured borehole foliations dip to the east at shallow angles can be explained by the fact that the metamorphic layering does not contain such folds everywhere and the limbs of the folds are relatively long and primarily dip to the east.

Foliation-Parting Low-Angle Fractures

Most of the fractures delineated from OTV images of the eight open-borehole wells were considered parallel to foliation or foliation-parting fractures (fig. 7). These types of fractures, described in Williams and others (2005), are developed where the foliation fabric dip angle is low, generally 30° or less; these discontinuities can be enhanced by unloading through weathering at land surface. Of the more than 3,600 fractures measured from the OTV images collected from the eight wells, 56 percent are considered to have low dip angles (30° or less). These types of fractures are not as well represented in the surface geologic mapping data (Wooten and others, 2010) because of the sampling bias described above in A Note about Sampling Biases Inherent in the Borehole Surveys and the Surface Outcrop Measurements. During field geologic mapping by the NCGS, no distinction was made between foliation with or without partings; however, the low-angle joints measured primarily were subparallel to foliation.

Steeply Dipping Subsurface Fractures

Joint sets having dip angles greater than 60° were observed as part of the surface geologic mapping by Wooten and others (2010) and grouped into sets based on dominant strike azimuths. (Note: Groups included a strike azimuth range of 15° on either side.) An analysis of primary and secondary subsurface fractures that also had dip angles greater than 60° was made to evaluate the occurrence of similar features in the wells that were logged. Steeply dipping (greater than 60° dip angle) joint sets having the following strike azimuth groups were categorized: 85 and 265°, 55° and 235°, 25 and 205°, 175 and 355°, 145 and 325°, and 115 and 295° (Wooten and others, 2010). Recognizing that vertical boreholes tap steeply dipping features much less frequently than shallow-dipping features (such as foliation-parting fractures), a total of 272 steeply dipping fractures delineated from the wells were categorized into these surface joint groups. From the eight wells logged by the USGS, the dominant steeply dipping fracture strike azimuth group measured in the wells was 25 and 205° (fig. 5; table 4), which parallels regional foliation but has a steeper dip angle (Wooten and others, 2010). Secondary joint groups delineated in the wells were 175 and 355°, also parallel to regional foliation strike, and 115 and 295° (fig. 8), parallel to the MGFZ orientation (Wooten and others, 2010).

Straddle-Packer Sample Zone Fracture Orientations and Geologic Features

From the results of straddle-packer sampling (David Edgerton, Lockheed Corporation, written commun., July 2010), specific orientations of fracture zone groups where trichloroethylene (TCE) and toluene were detected were analyzed for strike azimuth (Appendix 3). The most commonly measured orientation of the fracture zones where these volatile organic compounds (VOCs) were detected are 20–30° and 350–360° (table 5). The 20–30° orientation is parallel to the dominant structural orientation for all subsurface features (foliation, lithologic contacts, and fractures) in all eight wells logged by the USGS as well as the fracture orientations reported from the four CTS wells (fig. 5). This orientation also is parallel to the dominant steeply dipping subsurface fracture set (table 4) and is subparallel to the dominant subsurface foliation orientation (table 3). These north-northeast-trending orientations are parallel to the regional foliation orientation as mapped by Wooten and others (2010) and the dominant subsurface foliation 10–20° and the larger set of all subsurface features (0–30°).

Structures parallel to the MGFZ joint features were observed in all of the wells sampled using the straddle-packer assembly (table 5). The fracture sets include Well 1 (288–298 ft bls), CHR (80–90 ft and 484–504 ft bls), AW-4 (115–121 ft bls), AW-5 (418–428 ft and 560–570 ft bls), ERT-7 (6–13 ft, 60–67 ft, and 80–86 ft bls) and Oaks-2 (64–70 ft bls, Appendix 3).

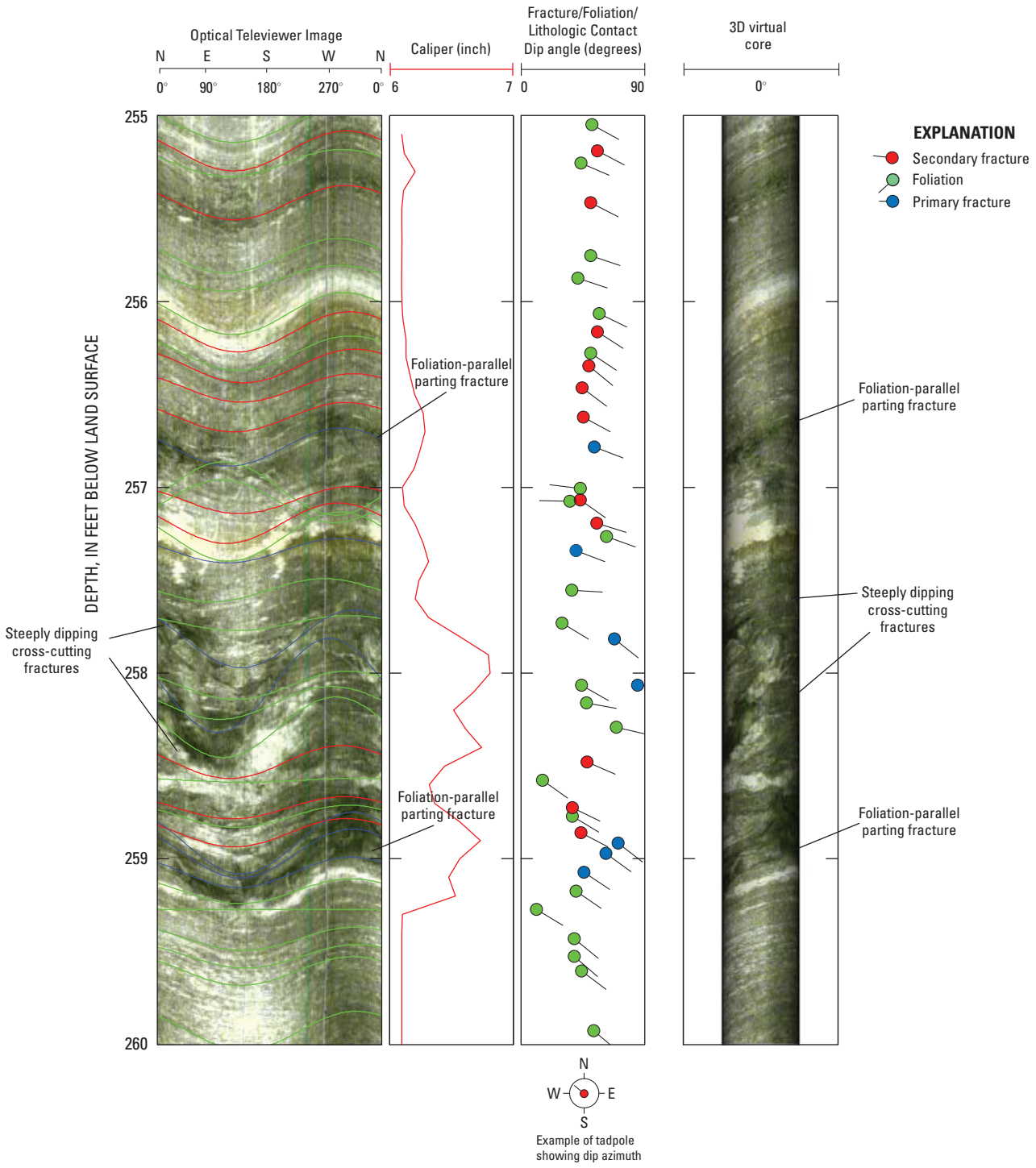

Figure 7. Optical televiewer image of Well 1 showing both low-angle foliation-parallel parting fractures and more steeply dipping cross-cutting fractures.

Table 4. Dominant strike azimuths of primary and secondary borehole fractures with dips of 60 degrees (°) or greater, categorized by surface geologic joint groups.

[See Appendix 2 for bar graphs of individual wells. MGFZ, parallel to Mills Gap Fault Zone structures]

Well number	Joint group strike azimuth group (+/–15°)					
	85° and 265° (MGFZ)	55° and 235°	25° and 205°	175° and 355°	145° and 325°	115° and 295° (MGFZ)
Well 1			X			
CHR						X
AW-4			X			
AW-5				X		
AW-7	X					
ERT-7			X			
Oaks-2			X			
ERT-6				X		

Note: Joint groups are centered on either side of the principle azimuth direction and include a range of 15° on either side. For example, 85° includes azimuths from 70° to 100°.

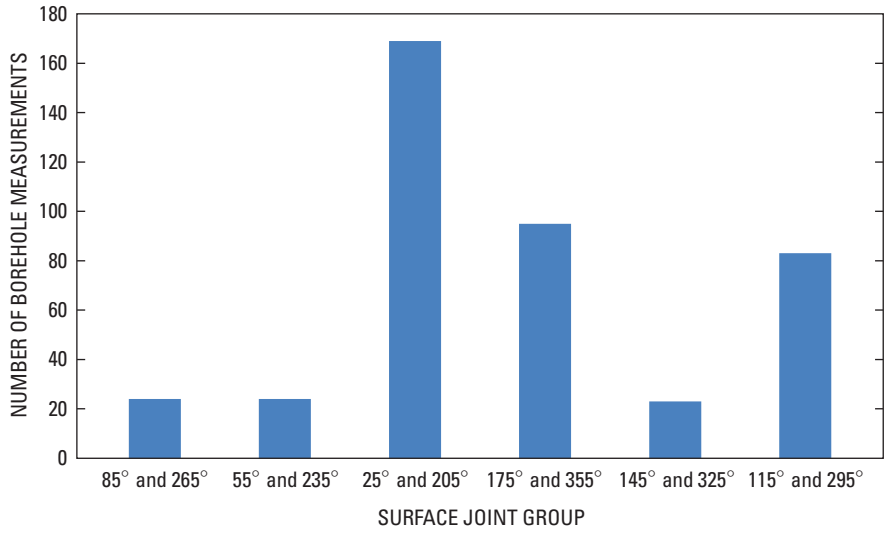

Figure 8. Strike azimuth of steeply dipping secondary fractures in wells categorized into surface joint groups.

Table 5. Listing of dominant fracture strike azimuth for packer depth intervals.

[Color designations correlate strike azimuth groups having the same bidirectional strike direction with opposite dip directions. >, greater than; MGFZ, parallel to Mills Gap Fault Zone structures; FP, foliation-parallel fracture; CC, cross-cutting fracture]

Well number	Packer depth interval (feet below land surface)	Fracture type (in order of prominence within the zone)	Fracture strike azimuth per 10-degree (°) bin (see rose diagrams in Appendix 3)															
			0–10°	>10–20°	>20–30°	>30–40°	>110–120° (MGFZ)	>180–190°	>200–210°	>210–220°	>220–230°	>270–280° (MGFZ)	>280–290° (MGFZ)	>300–310° (MGFZ)	>310–320°	>320–330°	>330–340°	>350–360°
Well 1	68–78	FP and CC	X															
	252–262	FP and CC			X													
	288–298	CC and FP					X										X	X
CHR	40–78	CC and FP		X														
	80–90	FP and CC	X	X									X					X
	484–504	FP and CC			X							X	X					
AW-4	115–121	CC and FP			X	X								X	X		X	X
	680–690	FP and CC	X															
AW-5	0–101	FP and CC			X													
	183–189	FP						X										
	200–210	FP and CC						X										
	418–428	FP and CC											X					
	560–570	FP and CC														X		
AW-7	53–58	FP and CC			X													
	88–94	FP and CC																X
	167–173	FP and CC																X
	229–239	FP and CC																X
	450–460	CC and FP															X	X
ERT-7	6–13	FP		X														
	60–67	FP		X														
	69–75	FP and CC	X		X				X							X	X	
	80–86	CC and FP									X							
Oaks-2	20–50	FP and CC		X														
	64–70	FP and CC			X					X								
	153–160	FP and CC				X												
	580–590	FP and CC				X												
Total number of zones			4	5	7	3	1	2	1	1	1	1	3	1	1	2	4	7

Note: 10° intervals not shown had no data population.

Three-dimensional views of fracture orientations where VOCs were detected are shown in figures 9, 10, and 11. Figure 9 is a view from east to west from wells CTS-MW-11B to Well 1, respectively. Figure 10 is a view from south to north from Well 1 to well CHR to well AW-4, respectively. Figure 11 is a view from west to east showing all six wells logged in the Oaks subdivision.

The cross sections shown as figures 12 and 13 (see fig. 1 for locations) depict measured subsurface features and surface geologic data in the areas of well locations. Depths to fracture zones and the associated TCE and toluene concentrations (David Edgerton, Lockheed Corporation, written commun., July 2010) are shown along with apparent dip angles and directions measured in the wells. Cross-section *A–A′* (fig. 12) depicts surface and subsurface measurements and geologic features (foliation, fractures, joint sets) from the CTS site (Marv Gobles, CTS Corporation, written commun., January 2010) to Well 1 in an easterly direction, parallel to the Mills Gap Fault structure and associated joint sets as mapped by Wooten and others (2010). Cross-section *B-B′* (fig. 13) depicts surface and subsurface measurements and geologic features from Well 1 to well AW-4 in a northeasterly direction, parallel to regional foliation strike and foliation-parallel joint sets as mapped by the NCGS and subsurface OTV interpretations of foliation orientation.

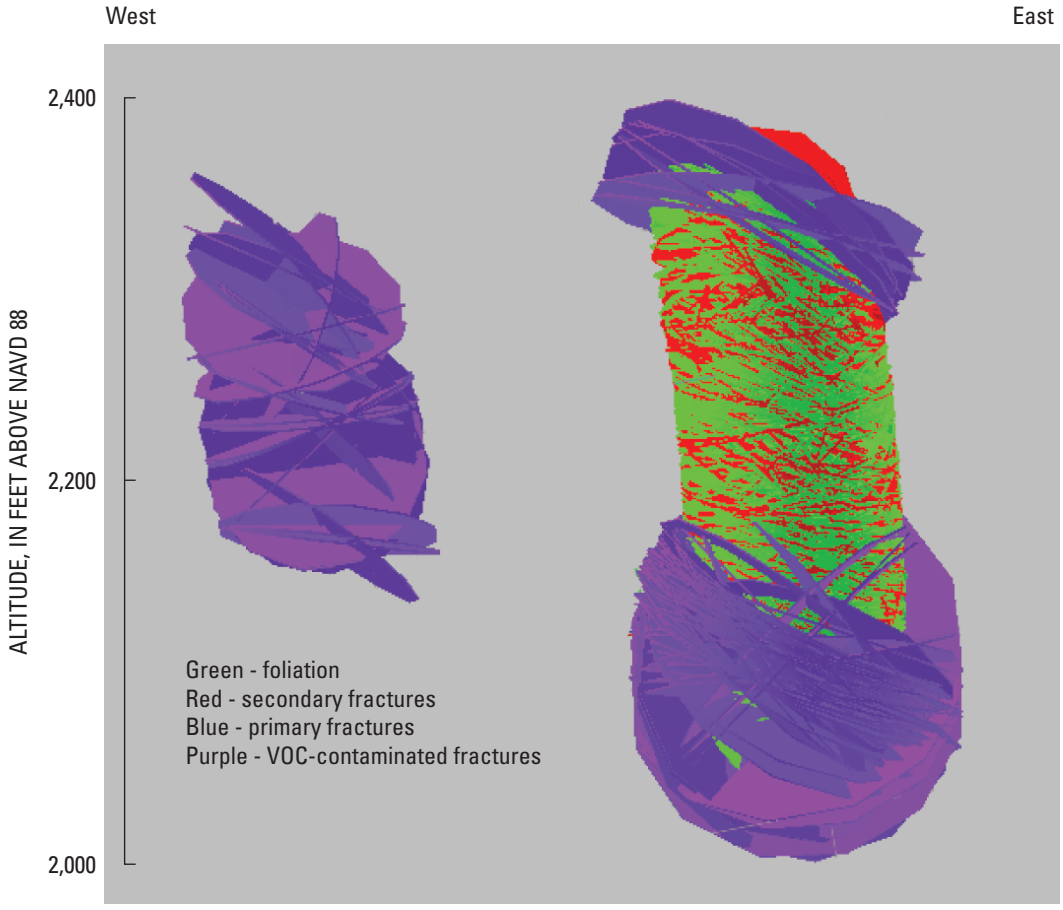

Figure 9. Three-dimensional view of VOC-contaminated fracture zones reported for well CTS-MW-11B and packer sampling in Well 1.

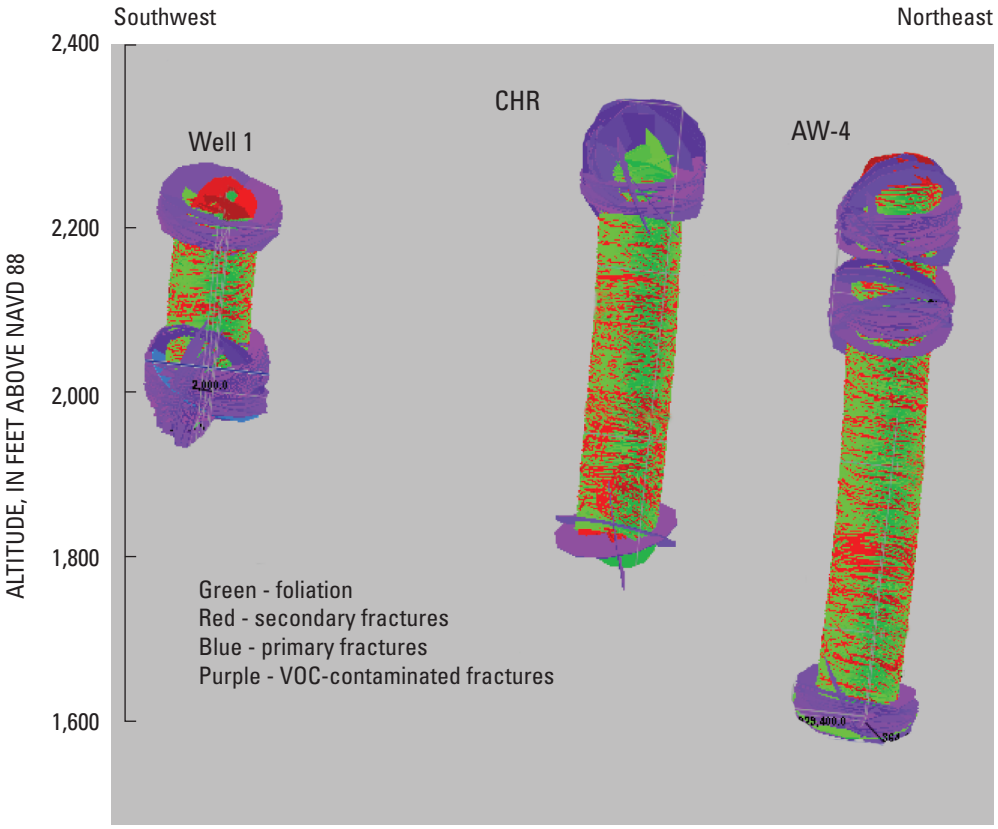

Figure 10. Three-dimensional view of VOC-contaminated fracture zones (from packer sampling) for Well 1, well CHR, and well AW-4.

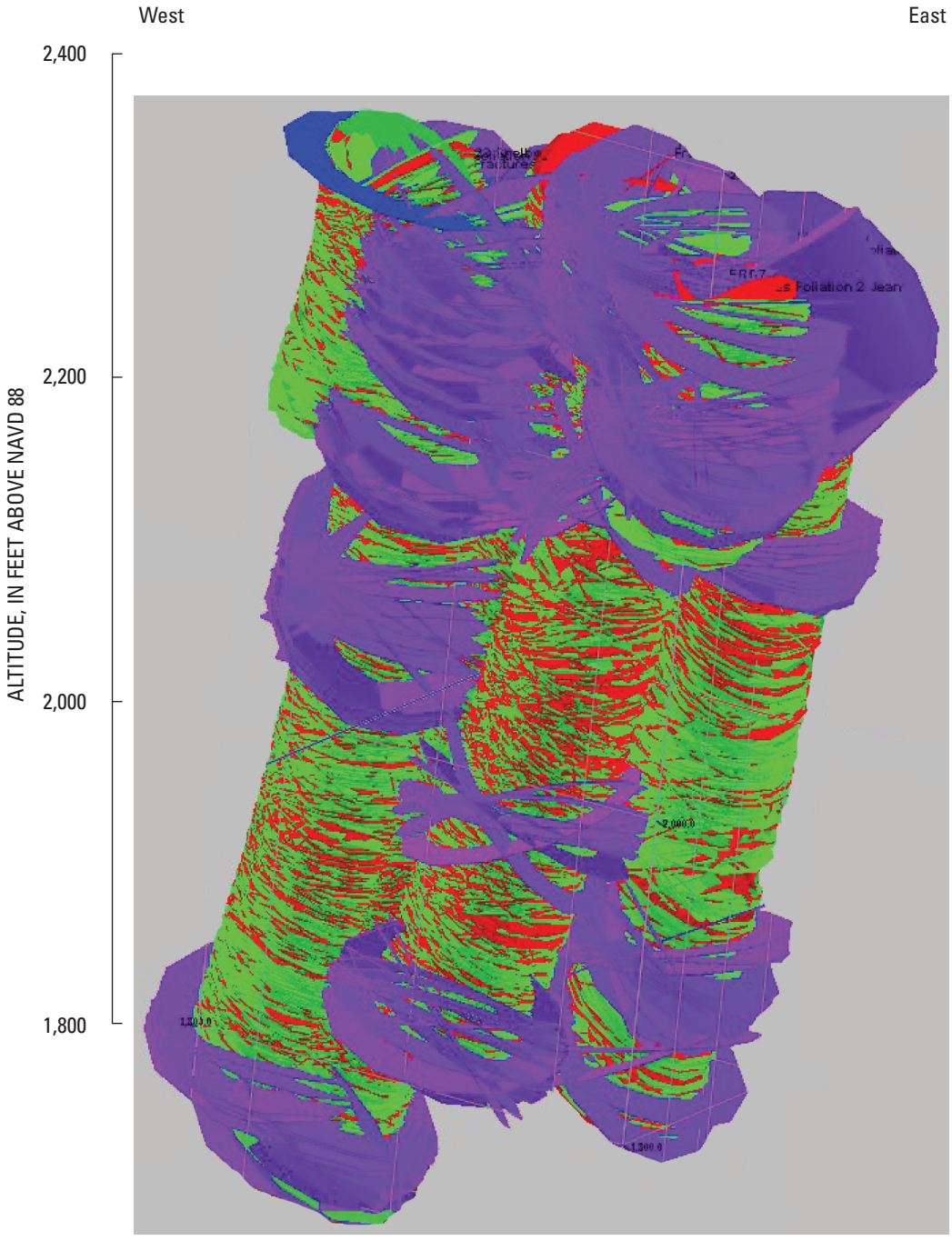

Figure 11. Three-dimensional view of VOC-contaminated fracture zones (from packer sampling) for the six Oaks wells.

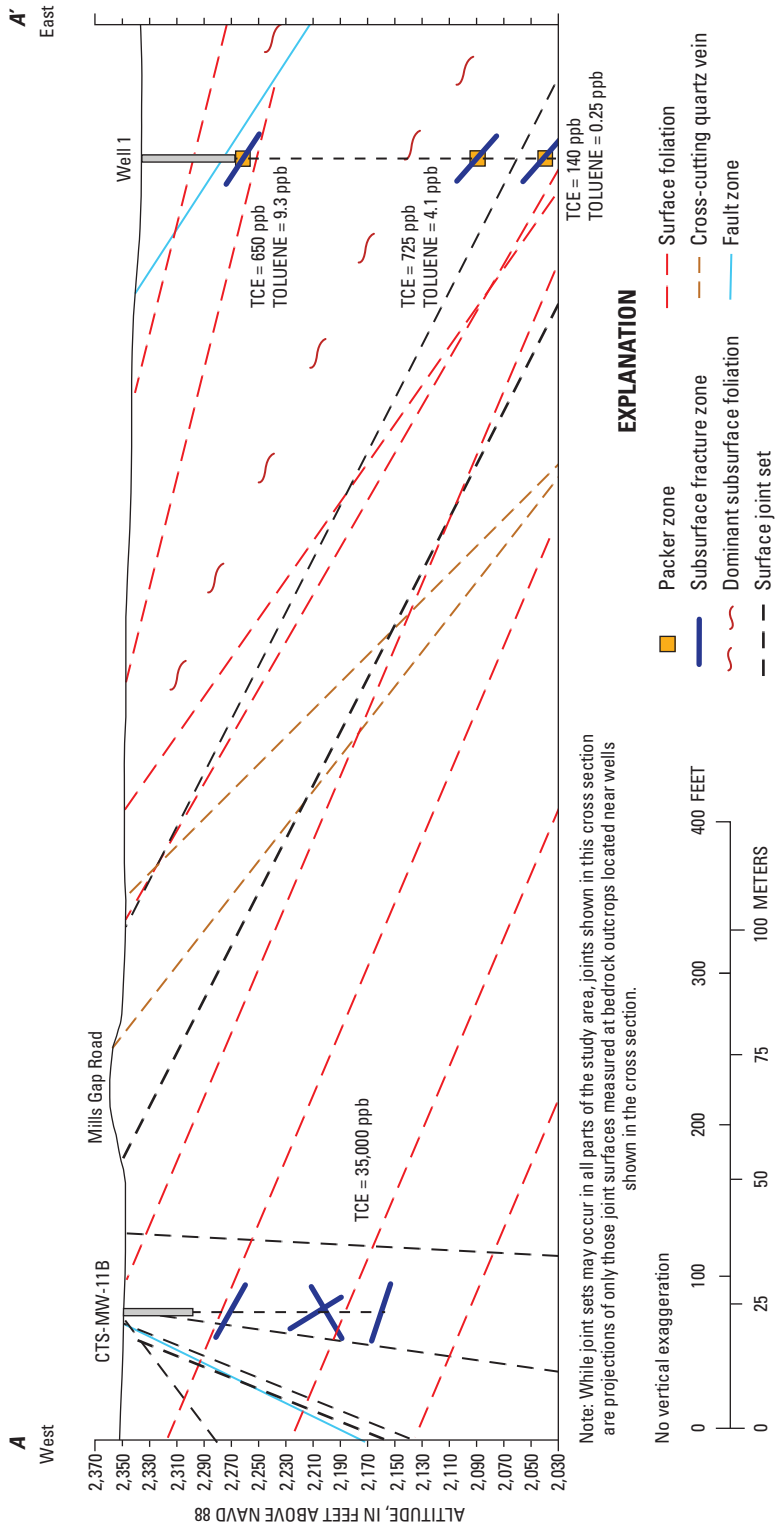

Figure 12. Schematic cross section (*A*–*A'*) showing depths to borehole fractures and detected trichloroethylene (TCE) and toluene concentrations, orientations of fractures, and geologic features from well CTS-MW-11B (west) to Well 1 (east).

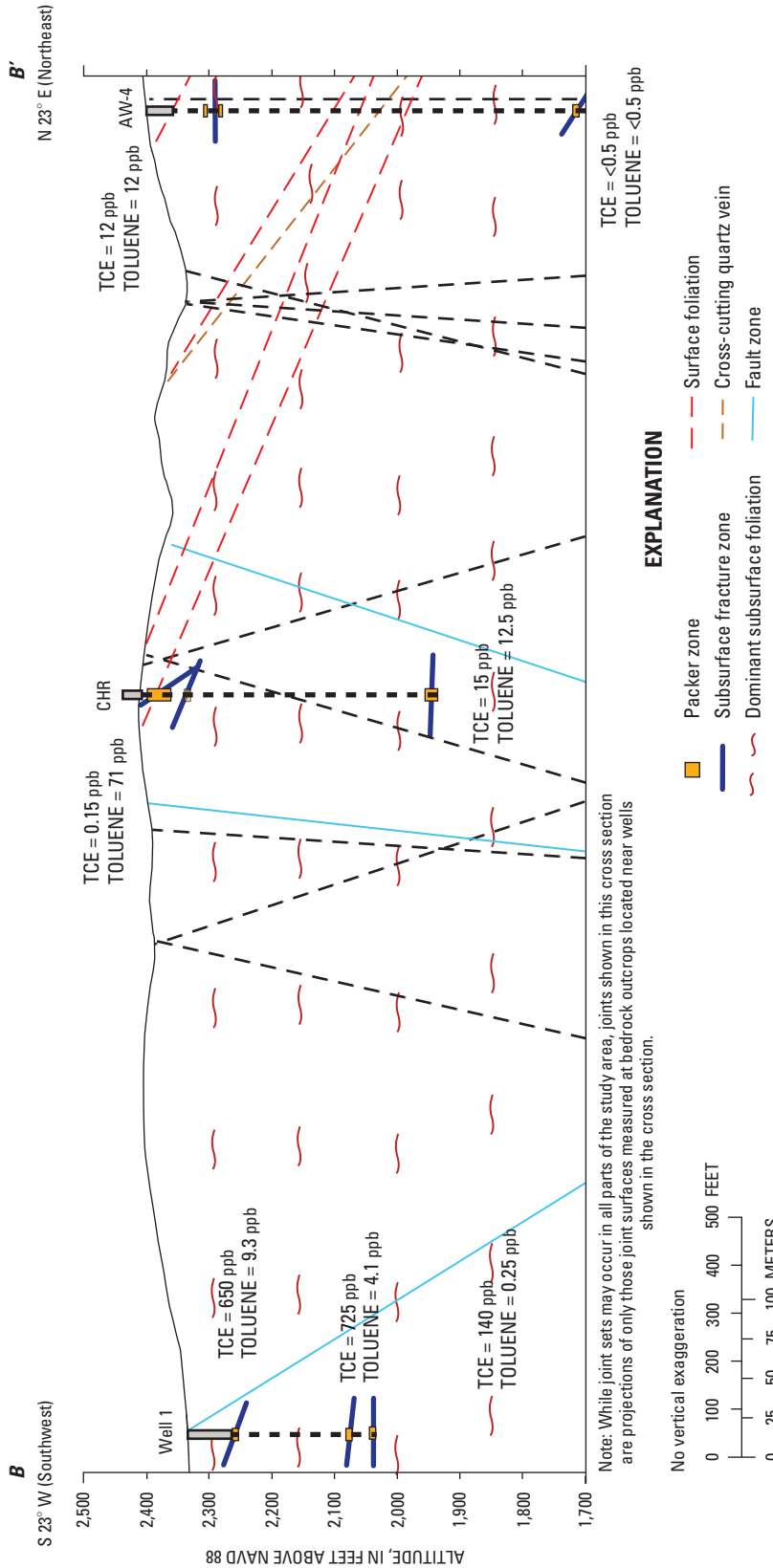

Figure 13. Schematic cross section (*B–B′*) showing depths to borehole fractures and detected trichloroethylene (TCE) and toluene concentrations, orientations of fractures, and geologic features from Well 1 (southwest) through well CHR (projected location) to well AW-4 in the Oaks (northeast).

References

aLt [Advanced Logic Technology], 2010, WellCad®—The composite log package: accessed on (September 15, 2010) at *http://www.alt.lu/welcad.htm*.

Chapman, M.J., Bolich, R.E., and Huffman, B.A., 2005, Hydrogeologic setting, ground-water flow, and ground-water quality at the Lake Wheeler Road research station, 2001–03, North Carolina Piedmont and Mountains Resource Evaluation Program: U.S. Geological Survey Scientific Investigations Report 2005–5166, 85 p.

Heath, R.C., 1980, Basic elements of ground-water hydrology with reference to conditions in North Carolina: U.S. Geological Survey Open-File Report 80-44, 86 p.

Heath, R.C., 1983, Basic ground-water hydrology: U.S. Geological Survey Water-Supply Paper 2220, 84 p.

Heath, R.C., 1984, Ground-water regions of the United States: U.S. Geological Survey Water-Supply Paper 2242, 78 p.

Heath, R.C., 1994, Ground-water recharge in North Carolina: Raleigh, North Carolina Department of Environment, Health, and Natural Resources, Groundwater Section, Open-File Report, 52 p.

Heath, R.C., and Jennings, G.D., 1995, North Carolina groundwater basics, *in* Smutko, L.S., Danielson, L.E., and Jennings, G.D., eds., The North Carolina wellhead protection guidebook: Raleigh, North Carolina Department of Environment, Health, and Natural Resources, Division of Environmental Management, Groundwater Section, Section 3, p. 3-1–3-21; accessed in July 2005 at *http://www.deh.enr.state.nc.us/pws/wellhead/update/wellhead_protection_program.htm* .

MACTEC Engineering and Consulting, Inc., Asheville, North Carolina, 2009, Report of Phase 1 Remedial Investigation, for the Mills Gap Road Site: prepared for the North Carolina Department of Environment and Natural Resources Division of Waste Management; accessed on September 24, 2010 at *http://portal.ncdenr.org/web/wm/sf/ctsmillsgap*.

Rockware, Inc., 2010, RockWorks™ earth science and GIS software: accessed on (September 24, 2010) at *http://www.rockware.com/*.

Williams, L.J., Kath, R.L., Crawford, T.J., and Chapman, M.J., 2005, Influence of geologic setting on ground-water availability in the Lawrenceville area, Gwinnett County, Georgia: U.S. Geological Survey Scientific Investigations Report 2005-5136, 43 p.

Wooten, R.M., Cattanach, B.L., Gillon, K.A., Bozdog, G.N., 2010, Geology of the Mills Gap area, Buncombe County, North Carolina: Report of Special Investigation 2010-09-30, Technical Memorandum to the U.S. Environmental Protection Agency, U.S. Geological Survey, and the North Carolina Department of Environment and Natural Resources Division of Waste Management, 19 p., 2 pls., map scale 1:12,000.

Appendix 1

A. Borehole geophysical logs showing fracture zones and vertical borehole flow:

Well 1
Well CHR
Well AW-4
Well AW-5
Well AW-7
Well ERT-7
Well Oaks-2
Well ERT-6

B. Optical televiewer images and structural orientations of foliation, lithologic contacts, and fractures:

Well 1
Well CHR
Well AW-4
Well AW-5
Well AW-7
Well ERT-7
Well Oaks-2
Well ERT-6

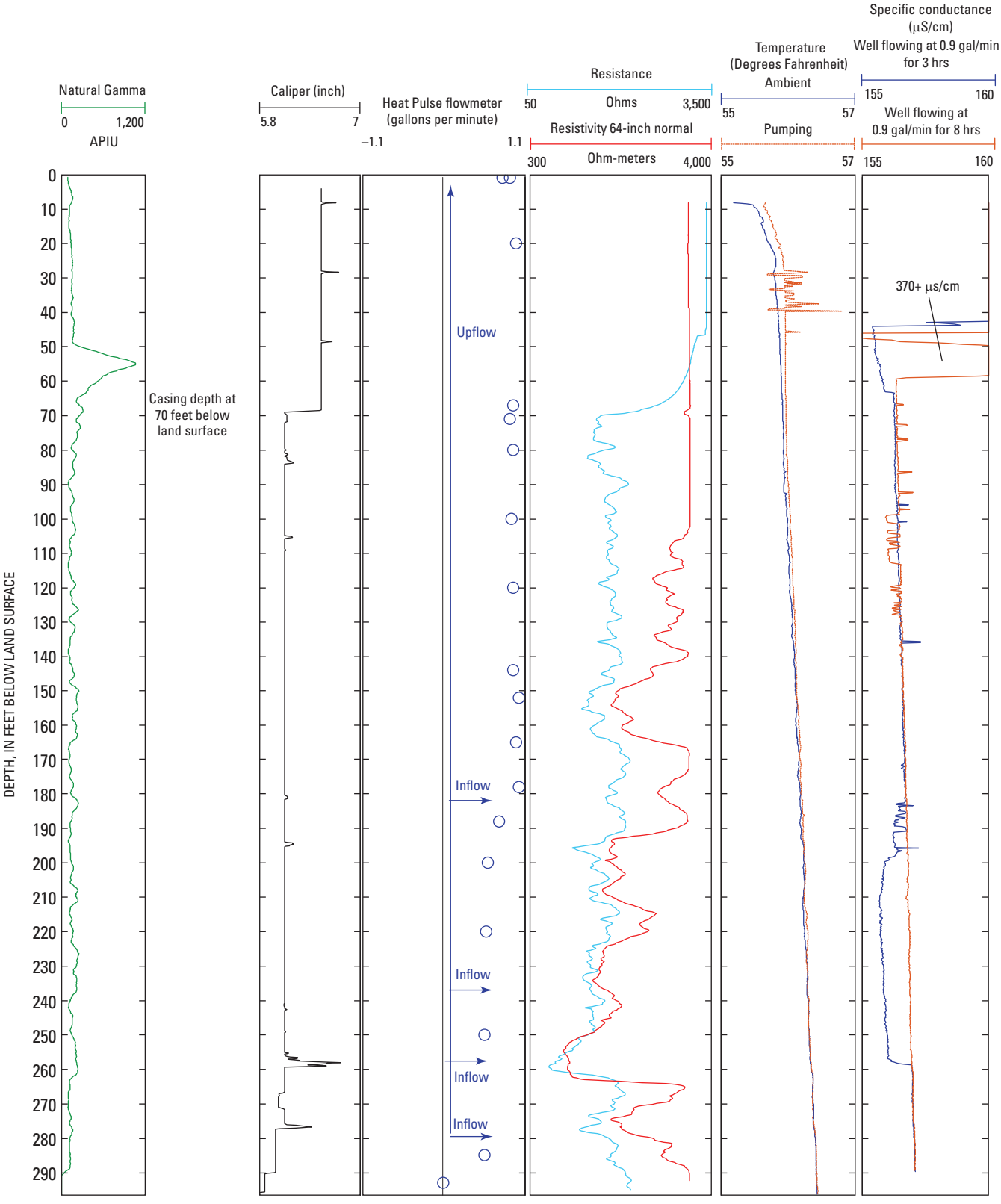

Appendix 1A. Borehole geophysical logs showing fracture zones and vertical borehole flow in Well 1.

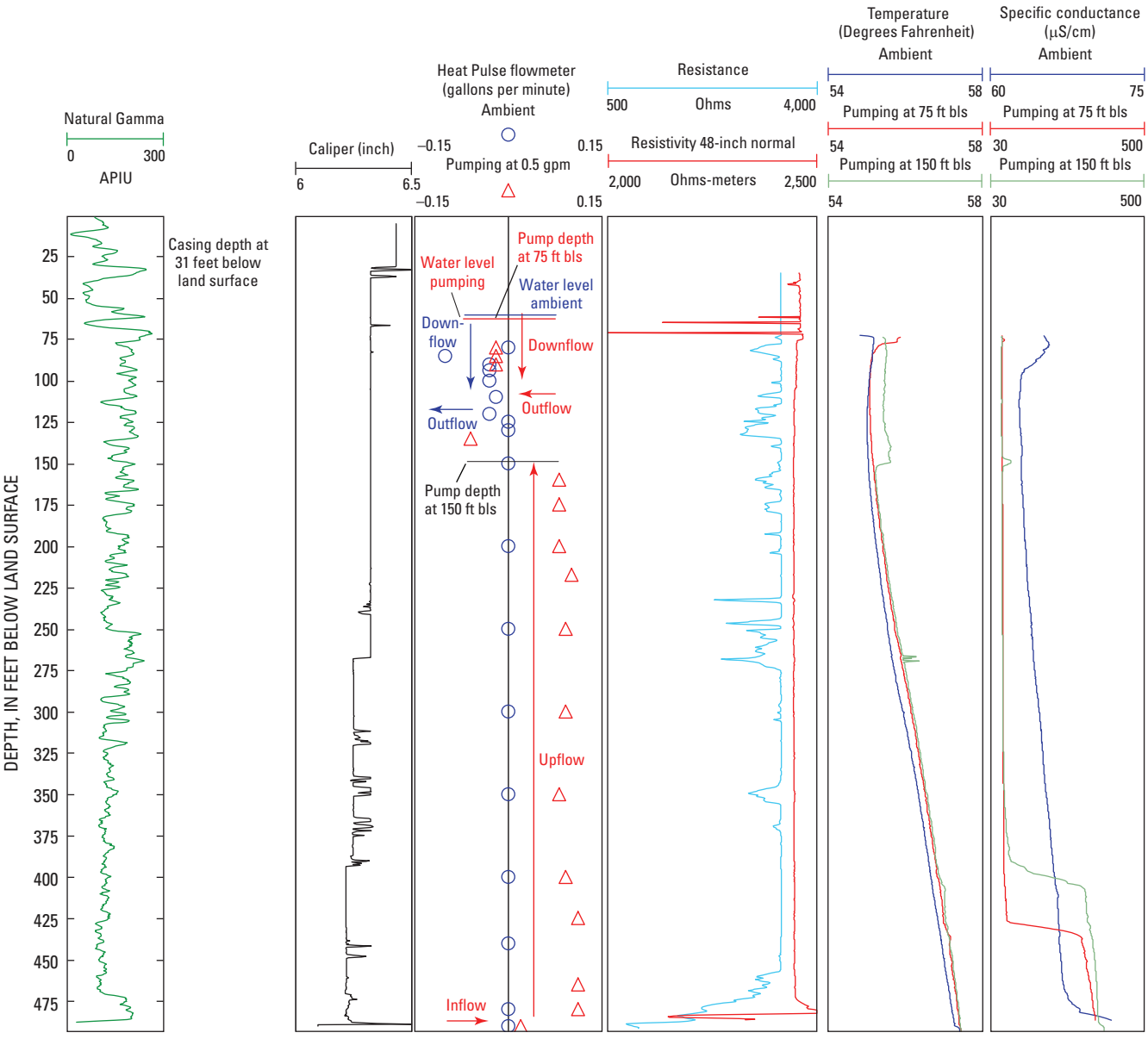

Appendix 1A. Borehole geophysical logs showing fracture zones and vertical borehole flow in well CHR.

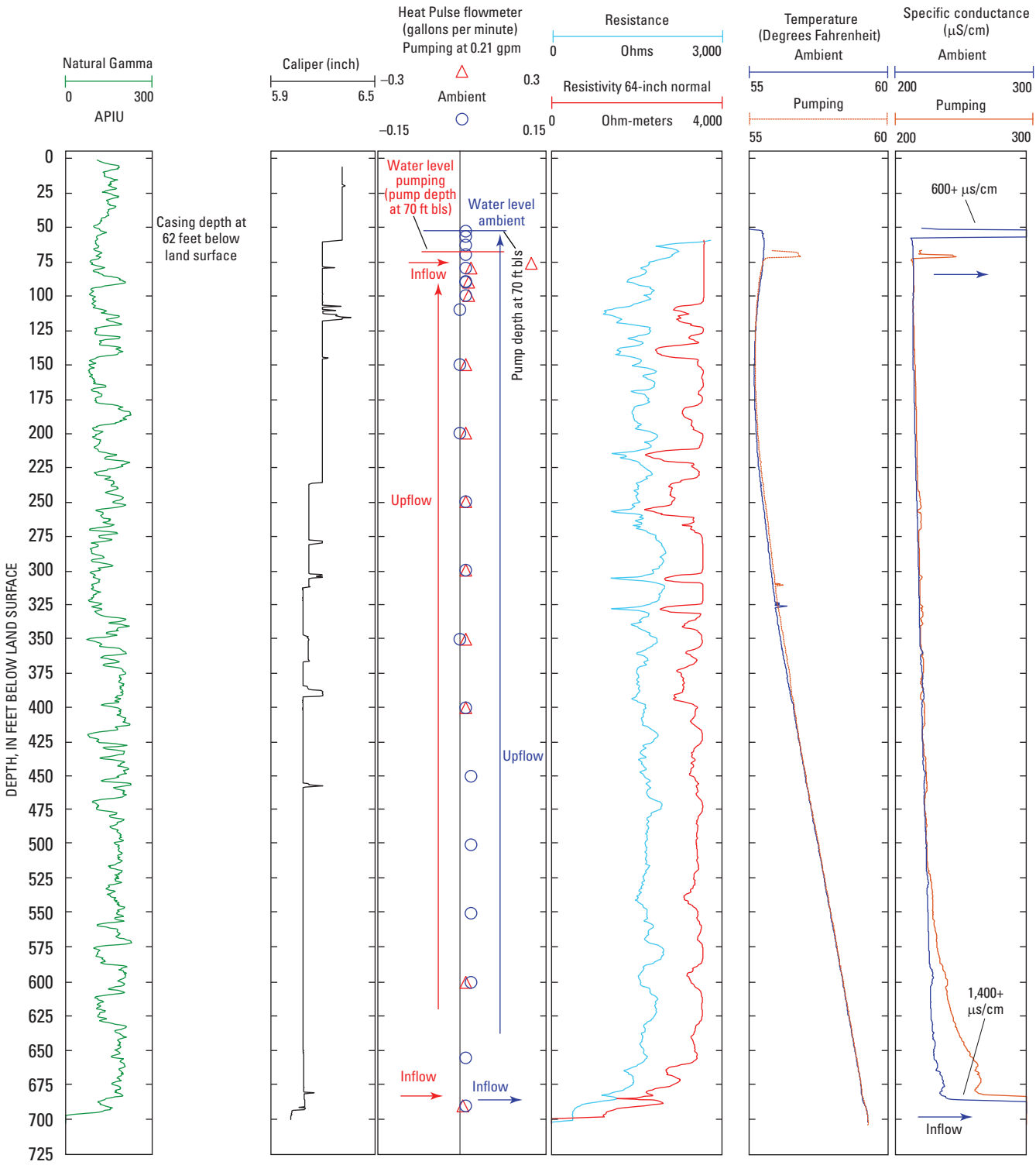

Appendix 1A. Borehole geophysical logs showing fracture zones and vertical borehole flow in well AW-4.

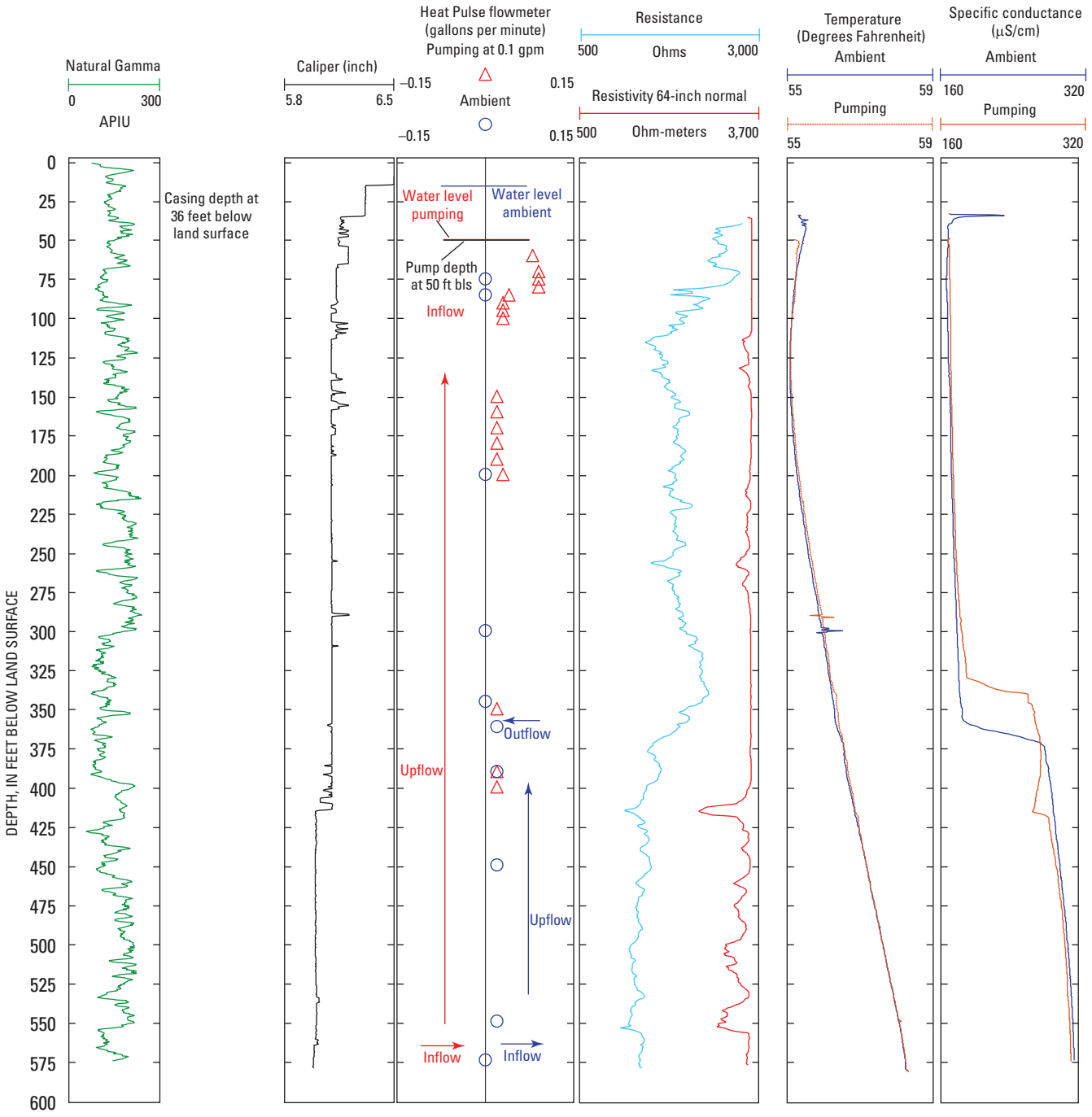

Appendix 1A. Borehole geophysical logs showing fracture zones and vertical borehole flow in well AW-5.

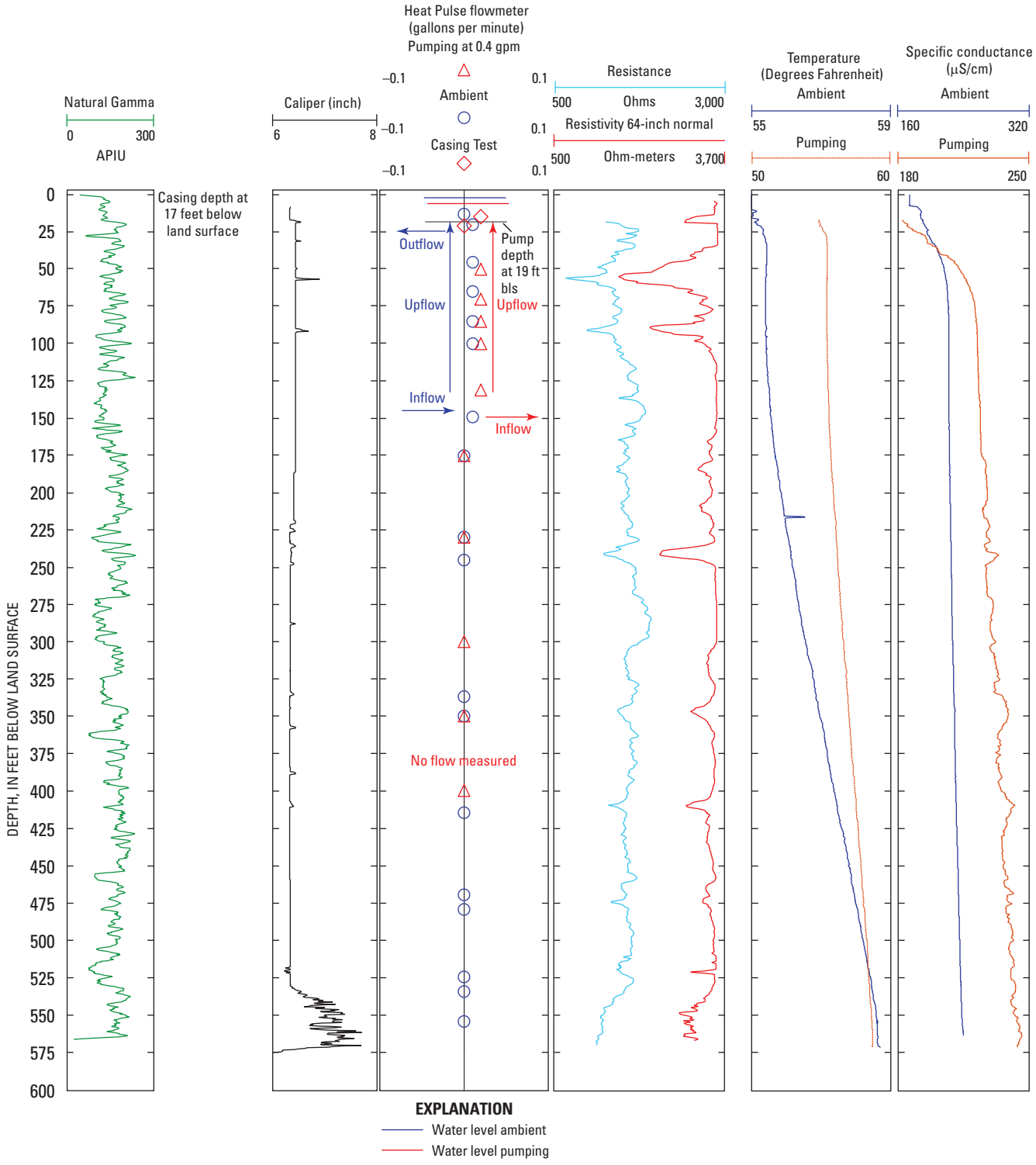

Appendix 1A. Borehole geophysical logs showing fracture zones and vertical borehole flow in well AW-7.

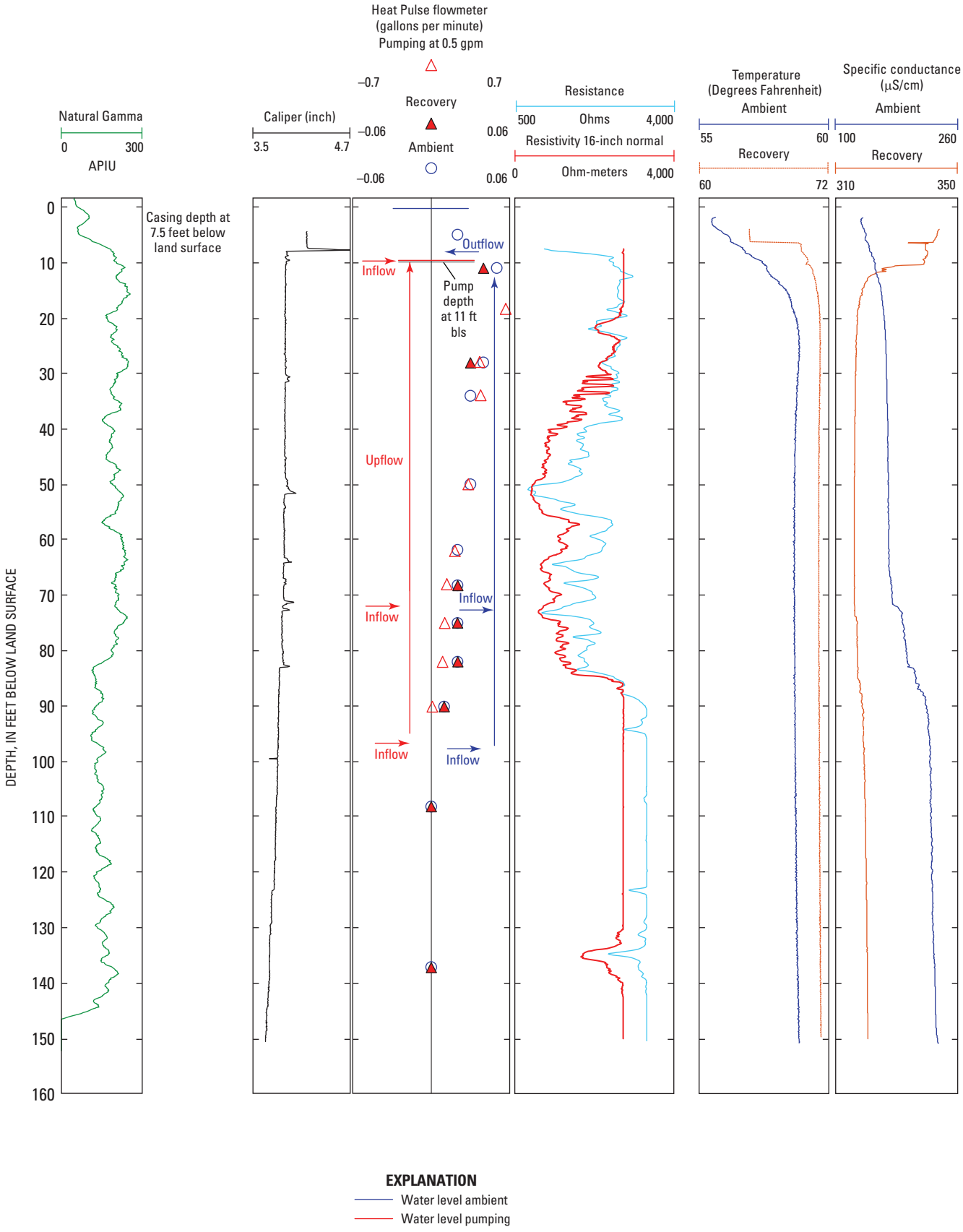

Appendix 1A. Borehole geophysical logs showing fracture zones and vertical borehole flow in well ERT-7.

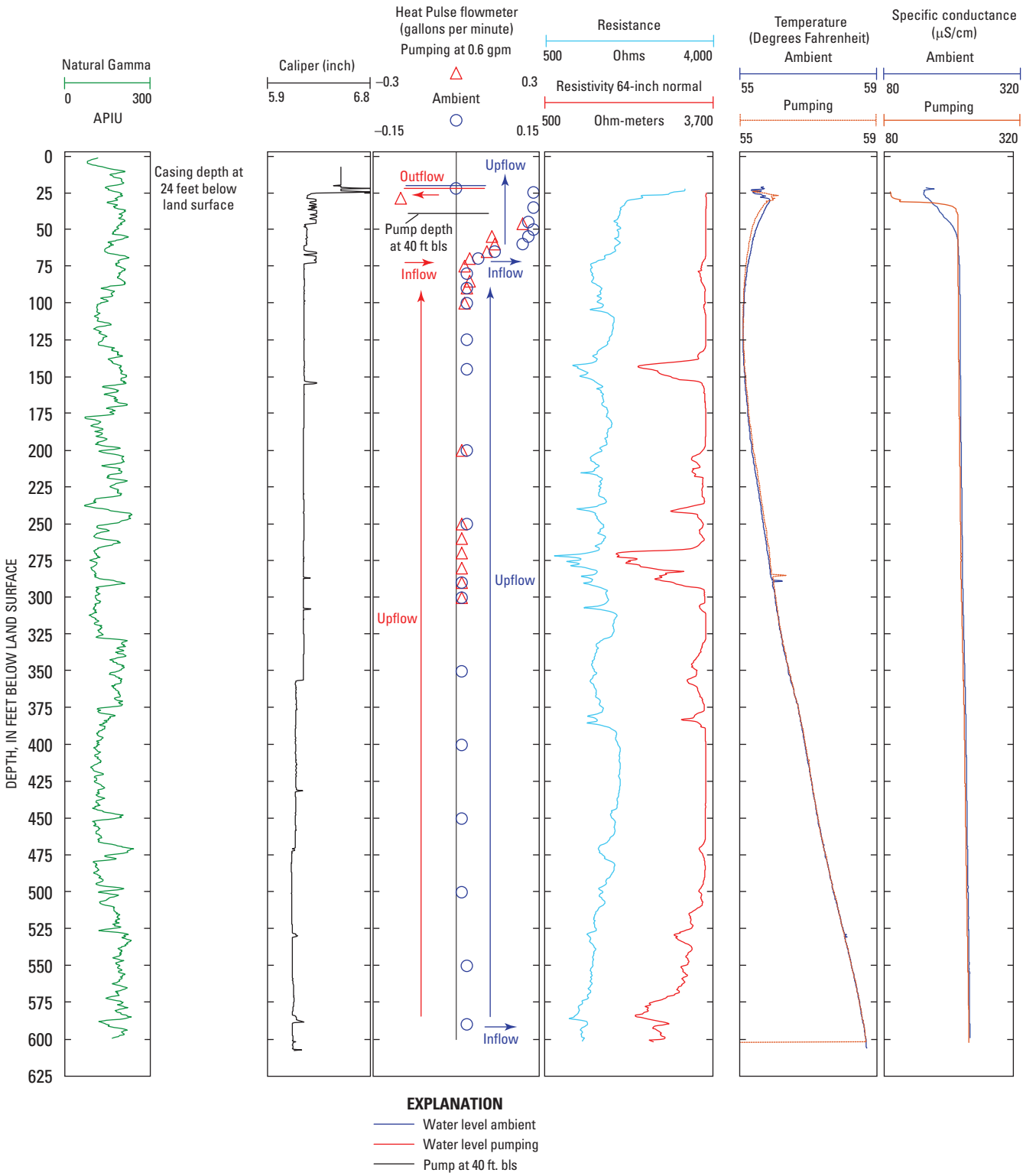

Appendix 1A. Borehole geophysical logs showing fracture zones and vertical borehole flow in well Oaks-2.

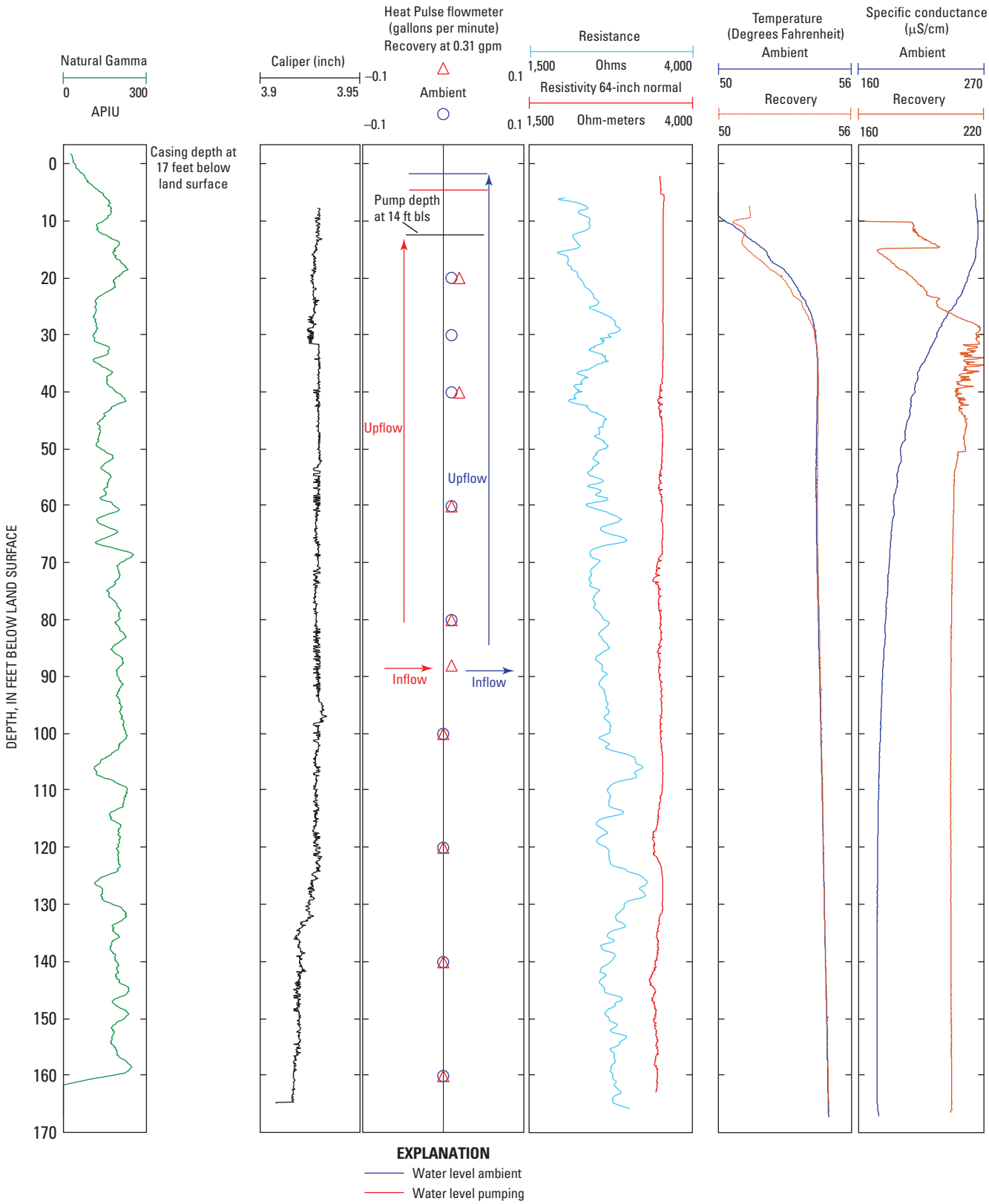

Appendix 1A. Borehole geophysical logs showing fracture zones and vertical borehole flow in well ERT-6.

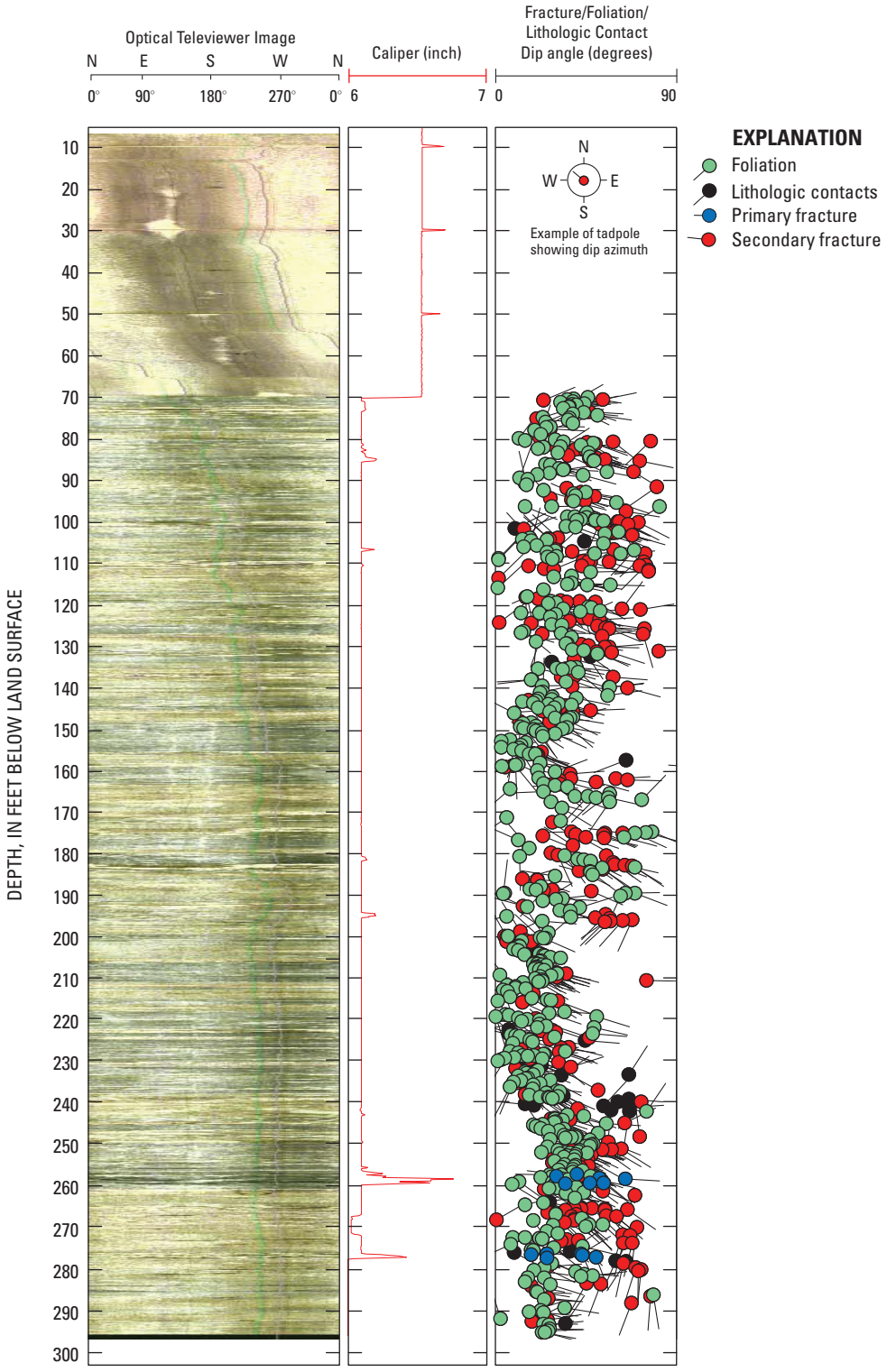

Appendix 1B. Optical televiewer images and structural orientations of foliation, lithologic contacts, and fractures in Well 1.

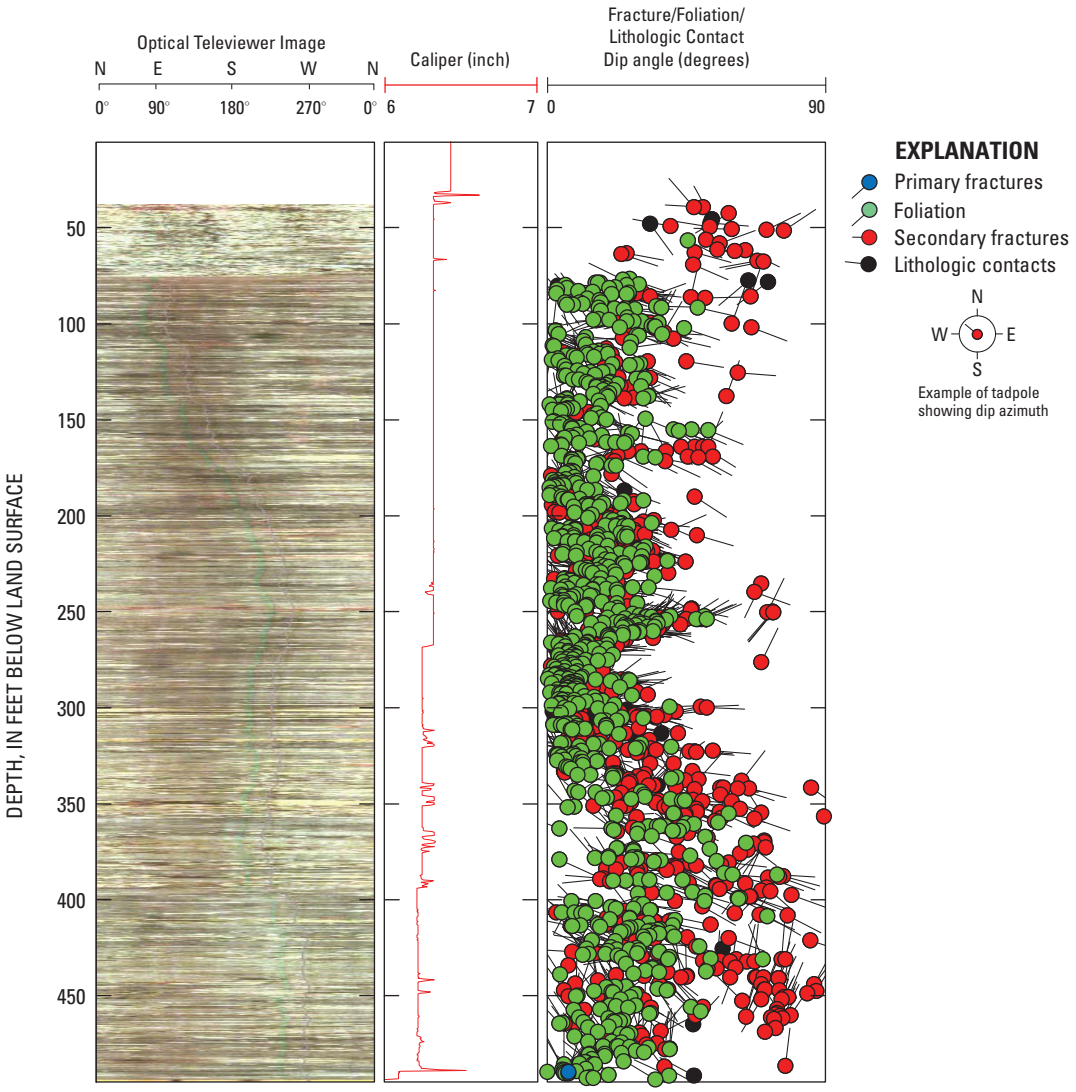

Appendix 1B. Optical televiewer images and structural orientations of foliation, lithologic contacts, and fractures in well CHR.

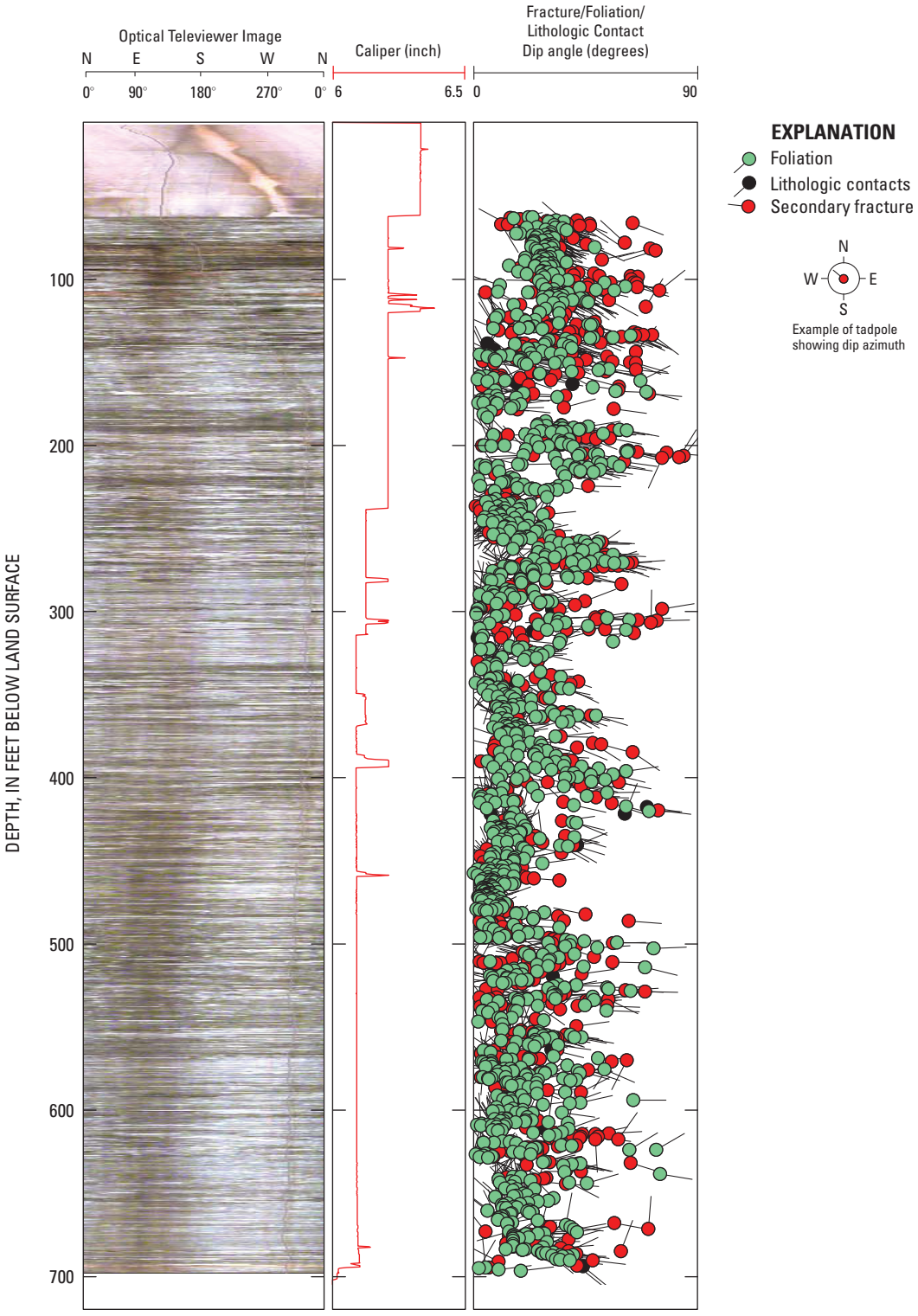

Appendix 1B. Optical televiewer images and structural orientations of foliation, lithologic contacts, and fractures in well AW-4.

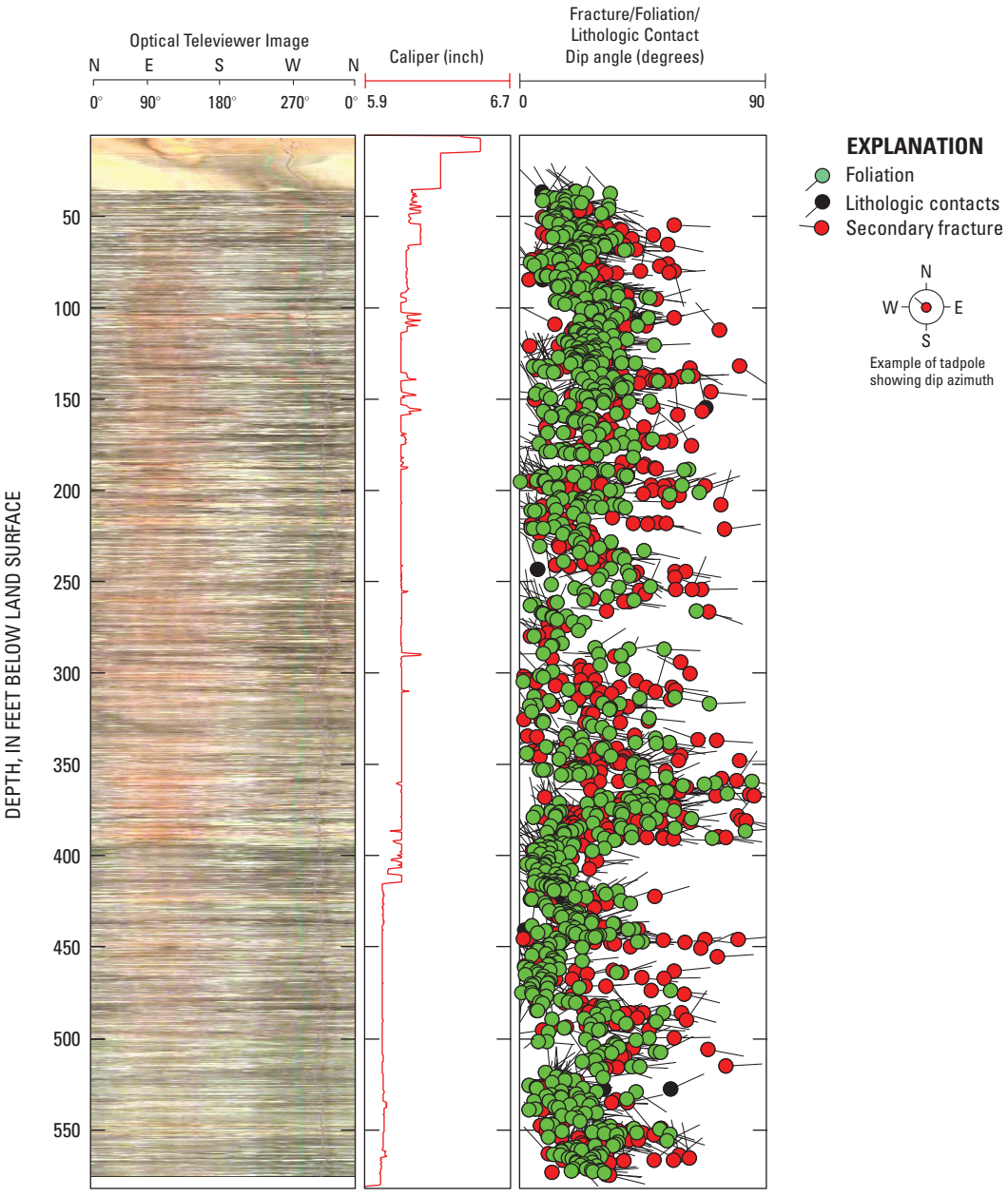

Appendix 1B. Optical televiewer images and structural orientations of foliation, lithologic contacts, and fractures in well AW-5.

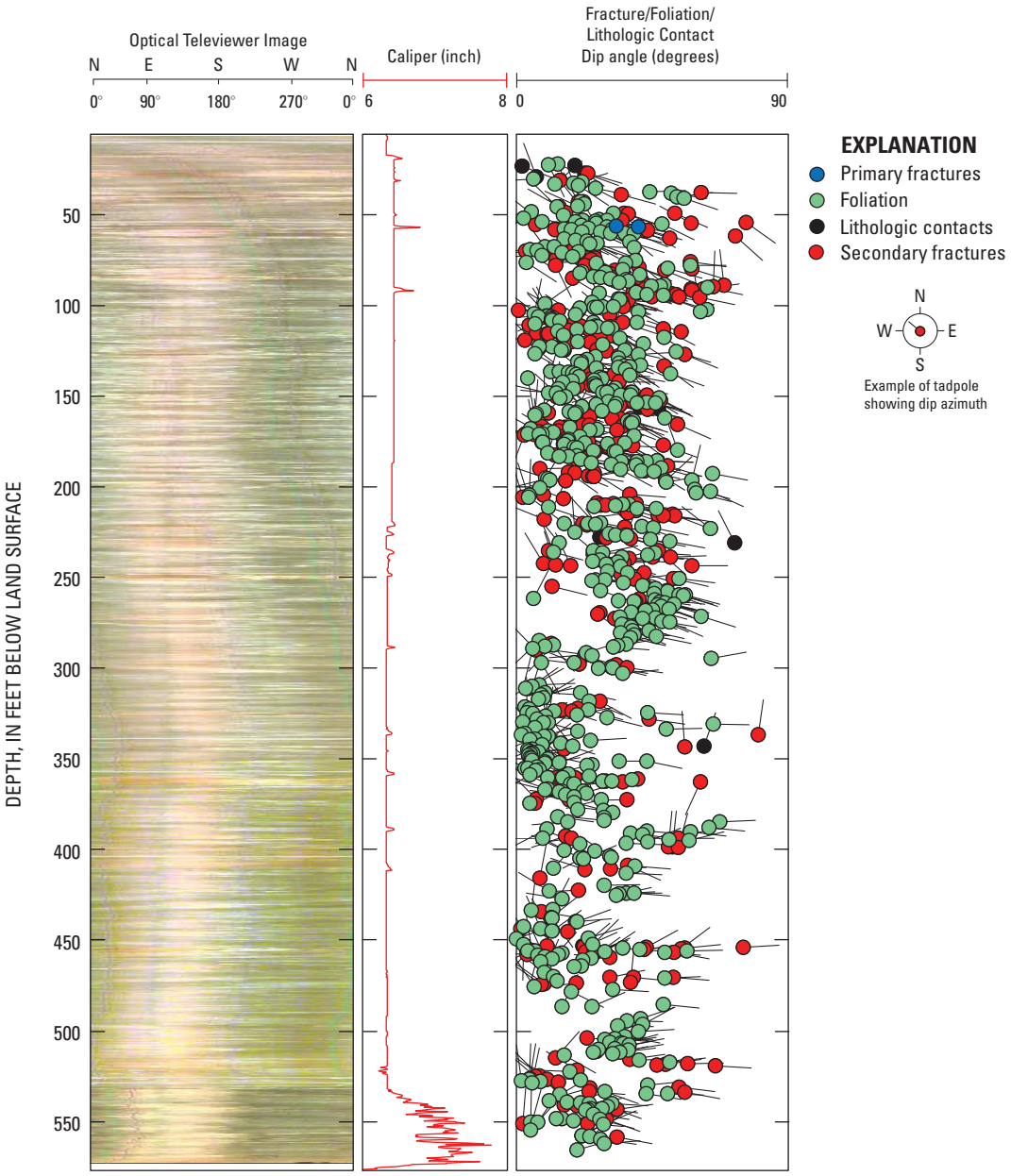

Appendix 1B. Optical televiewer images and structural orientations of foliation, lithologic contacts, and fractures in well AW-7.

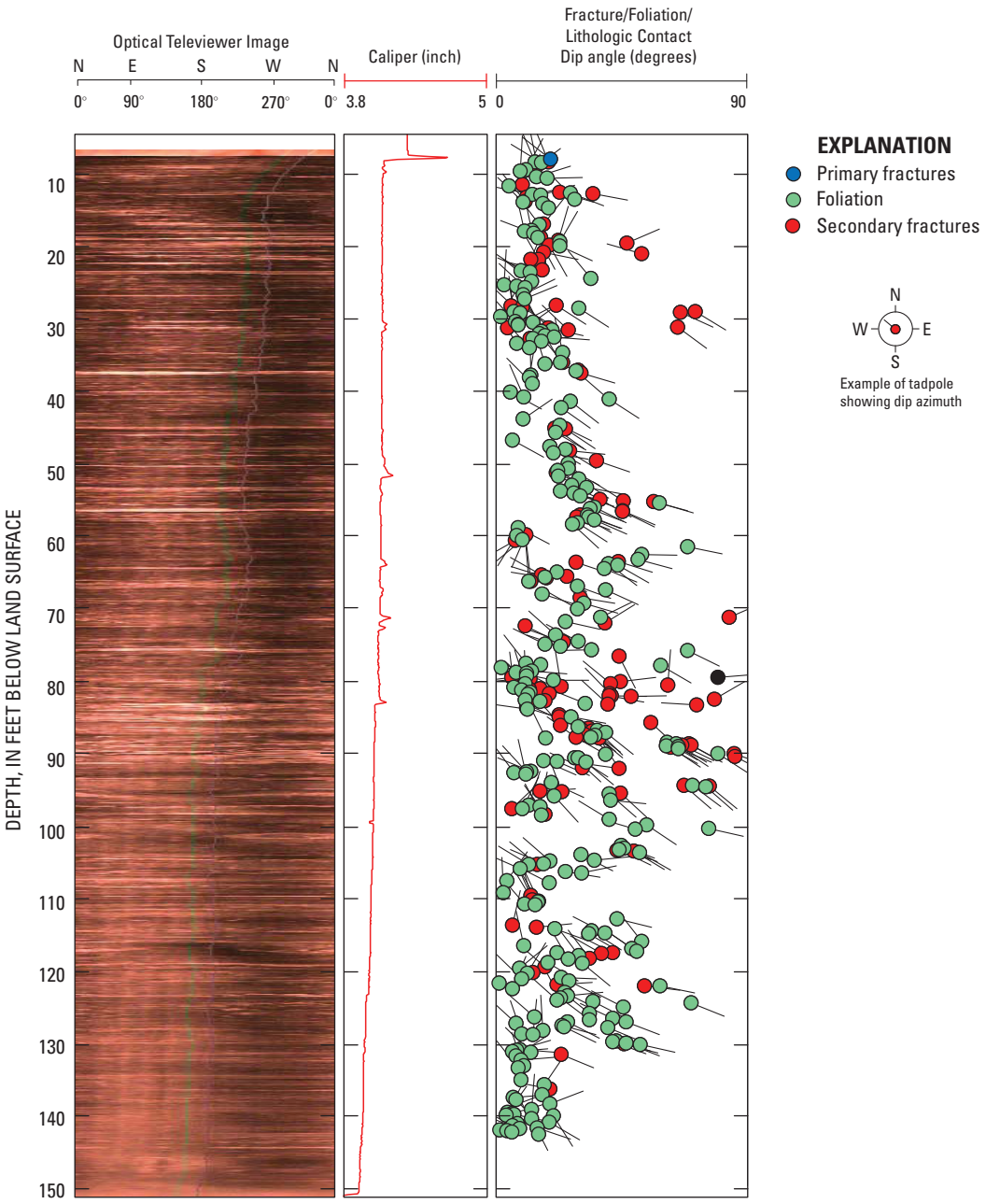

Appendix 1B. Optical televiewer images and structural orientations of foliation, lithologic contacts, and fractures in well ERT-7.

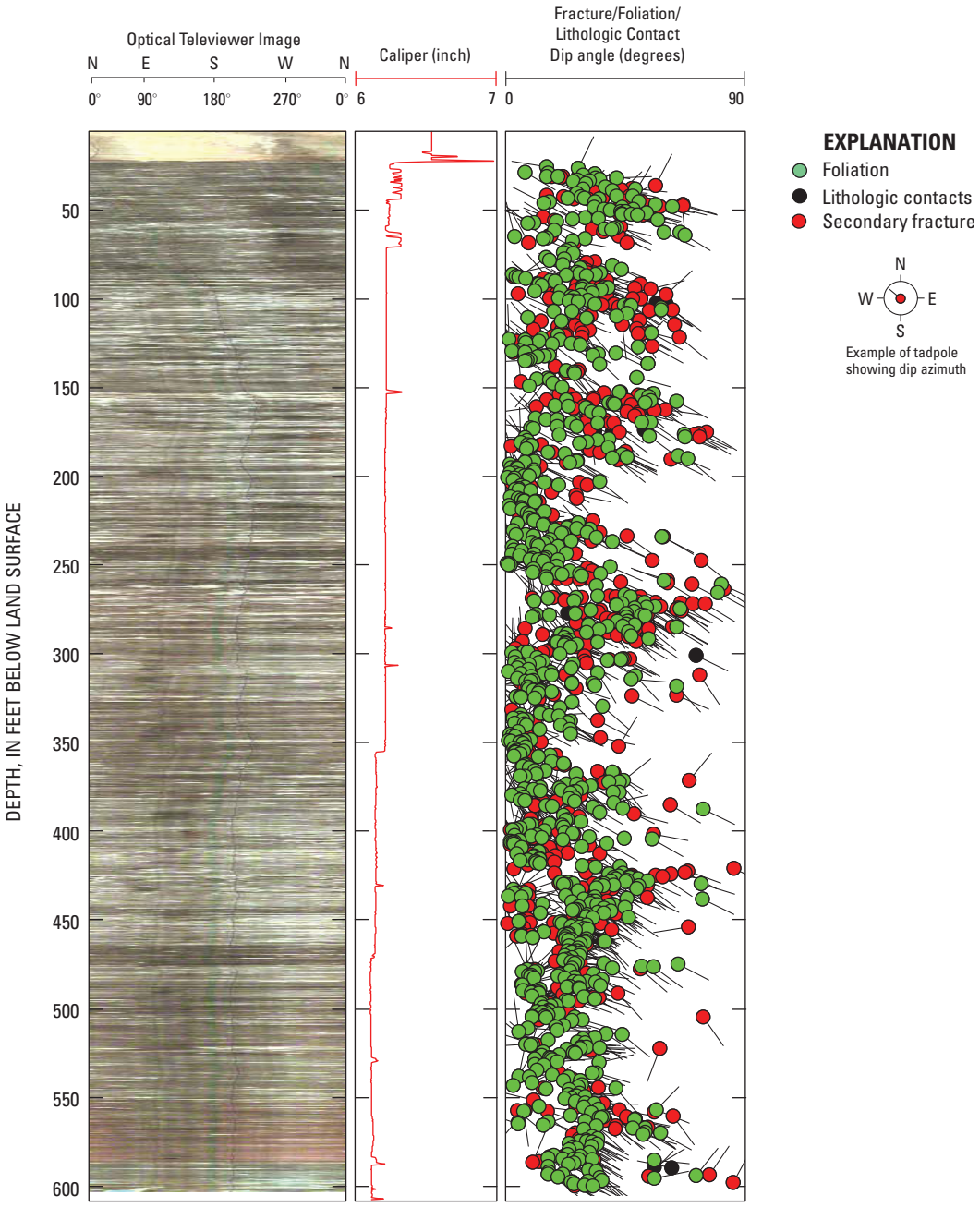

Appendix 1B. Optical televiewer images and structural orientations of foliation, lithologic contacts, and fractures in well Oaks-2.

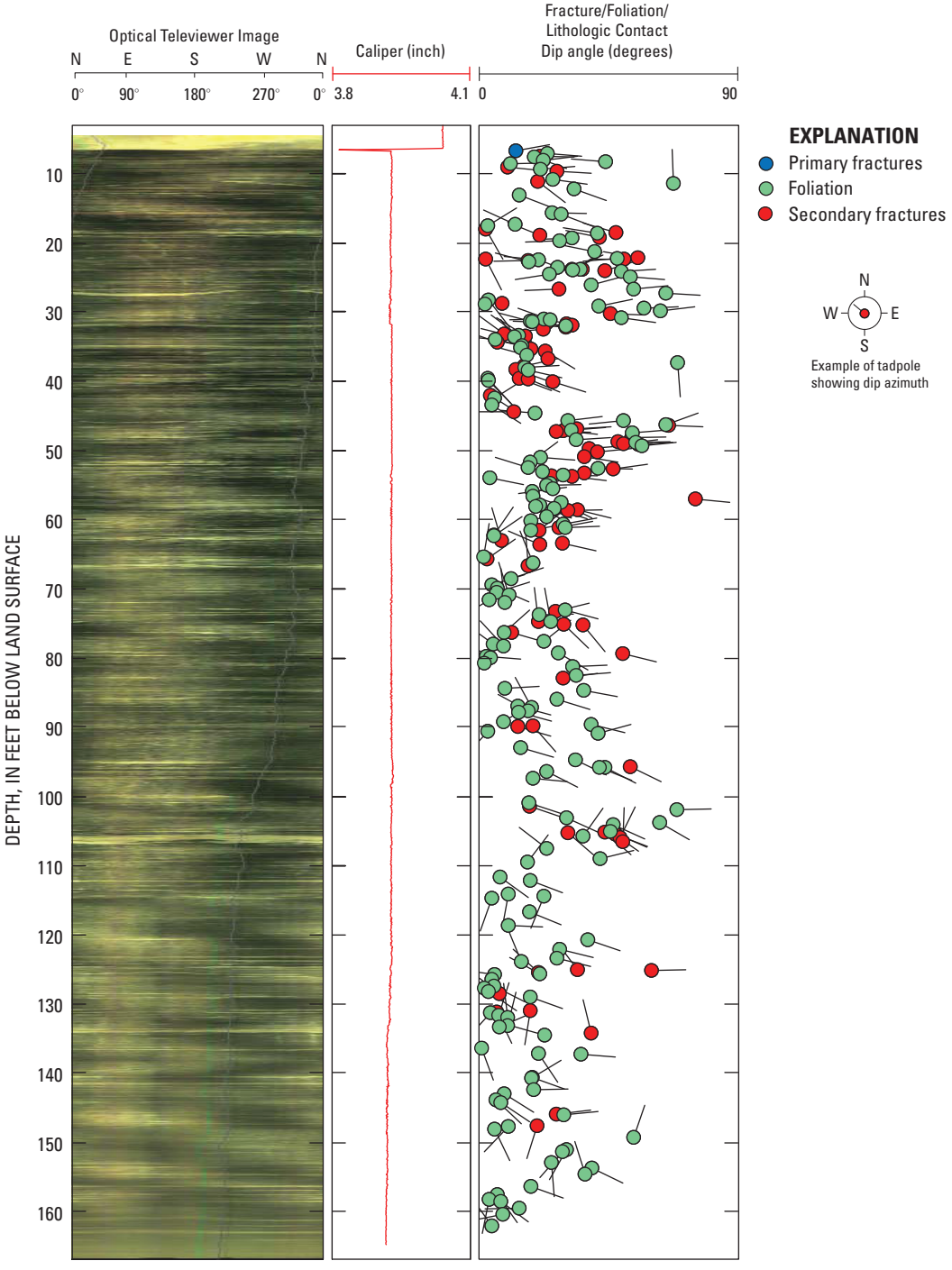

Appendix 1B. Optical televiewer images and structural orientations of foliation, lithologic contacts, and fractures in well ERT-6.

Appendix 2

Borehole foliation dip azimuth frequency distribution graphs as determined from optical televiewer images:

Well 1

Well CHR

Well AW-4

Well AW-5

Well AW-7

Well ERT-7

Well Oaks-2

Well ERT-6

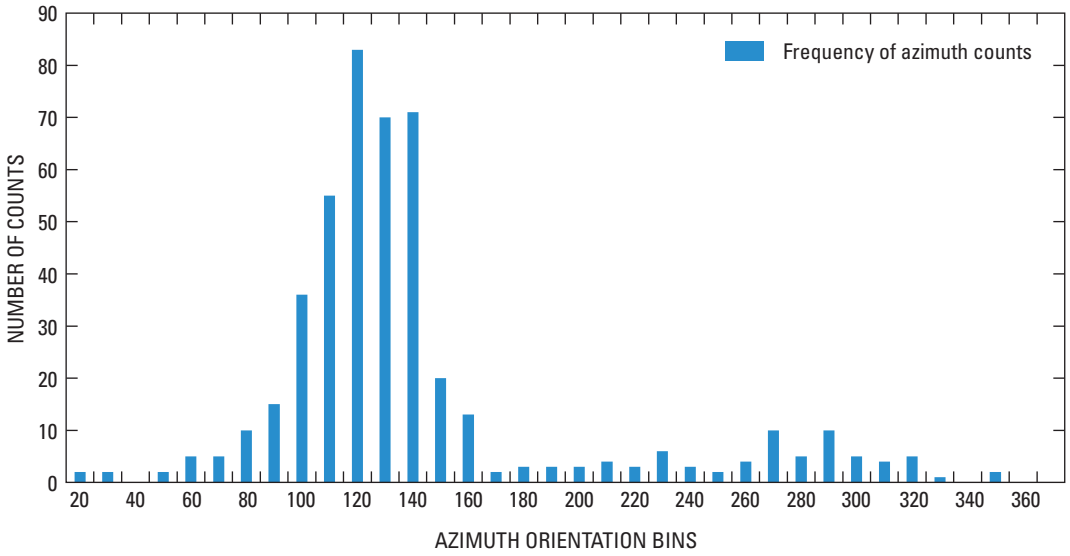

Appendix 2. Borehole foliation dip azimuth frequency distribution graphs as determined from optical televiewer images in Well 1.

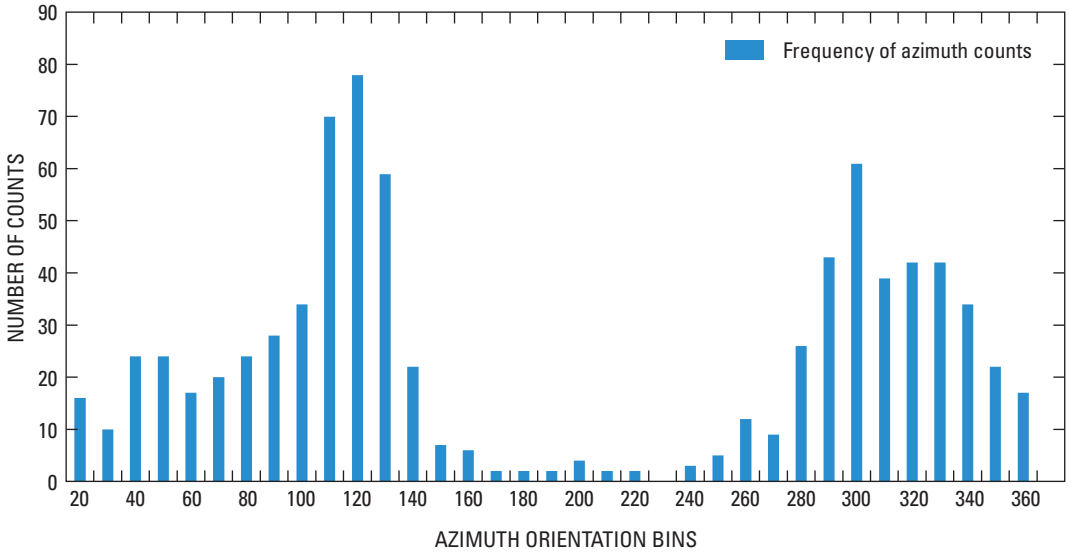

Appendix 2. Borehole foliation dip azimuth frequency distribution graphs as determined from optical televiewer images in well CHR.

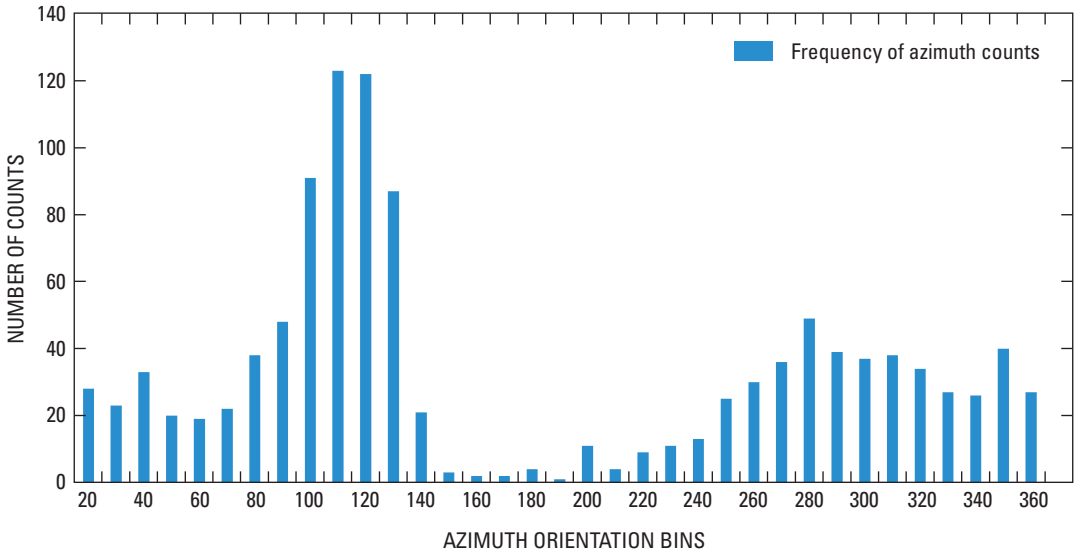

Appendix 2. Borehole foliation dip azimuth frequency distribution graphs as determined from optical televiewer images in well AW-4.

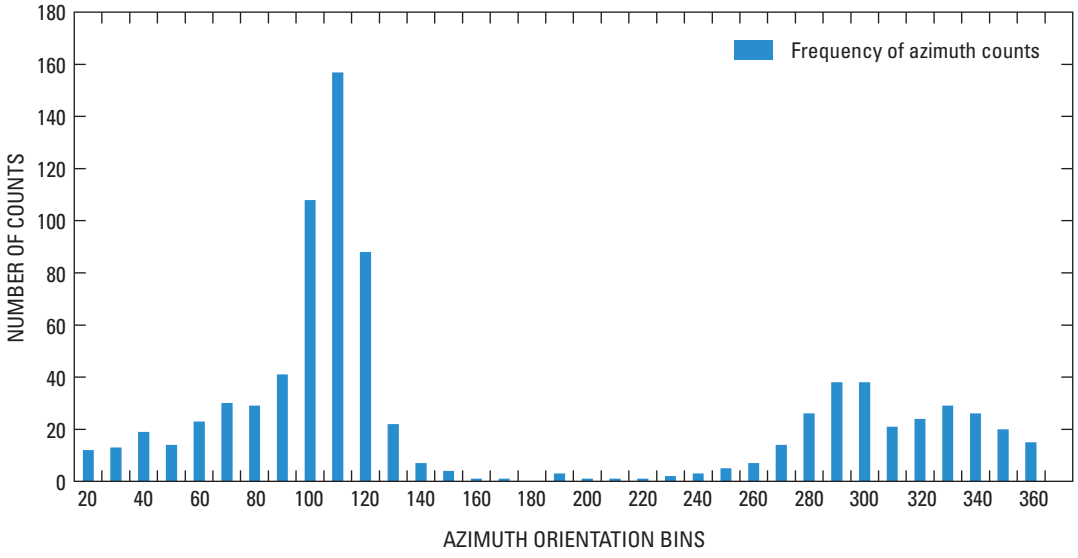

Appendix 2. Borehole foliation dip azimuth frequency distribution graphs as determined from optical televiewer images in well AW-5.

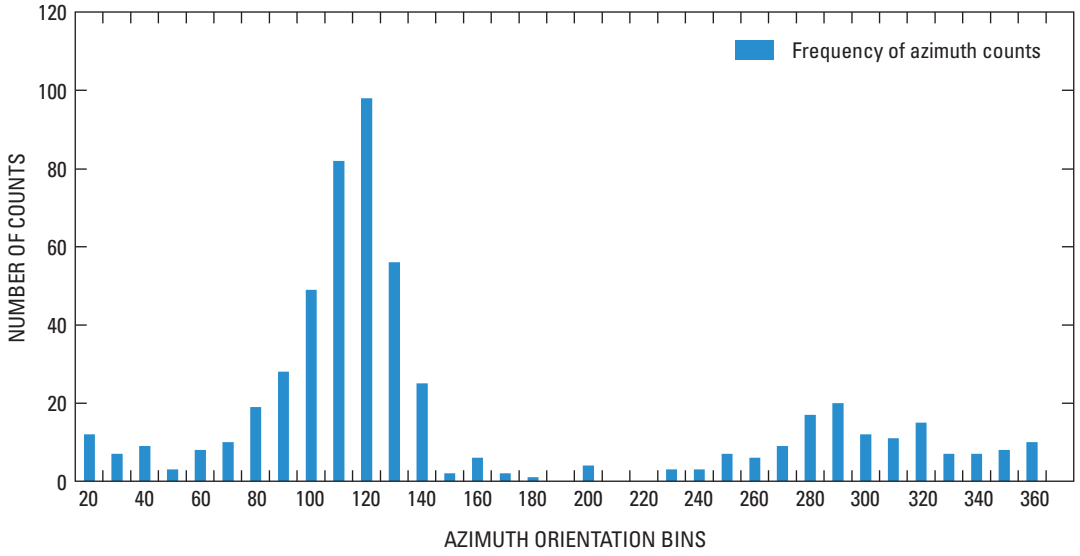

Appendix 2. Borehole foliation dip azimuth frequency distribution graphs as determined from optical televiewer images in well AW-7.

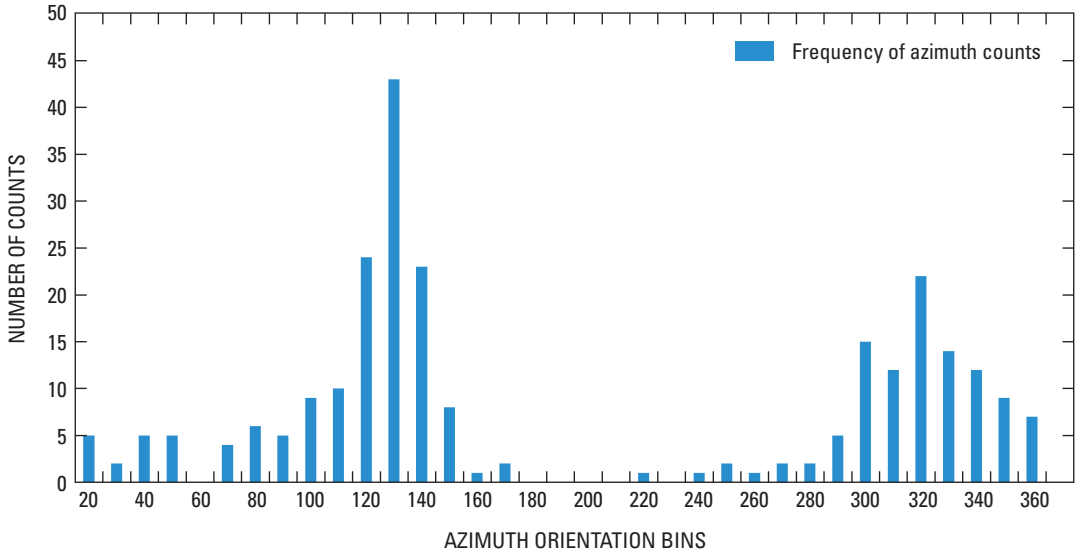

Appendix 2. Borehole foliation dip azimuth frequency distribution graphs as determined from optical televiewer images in well ERT-7.

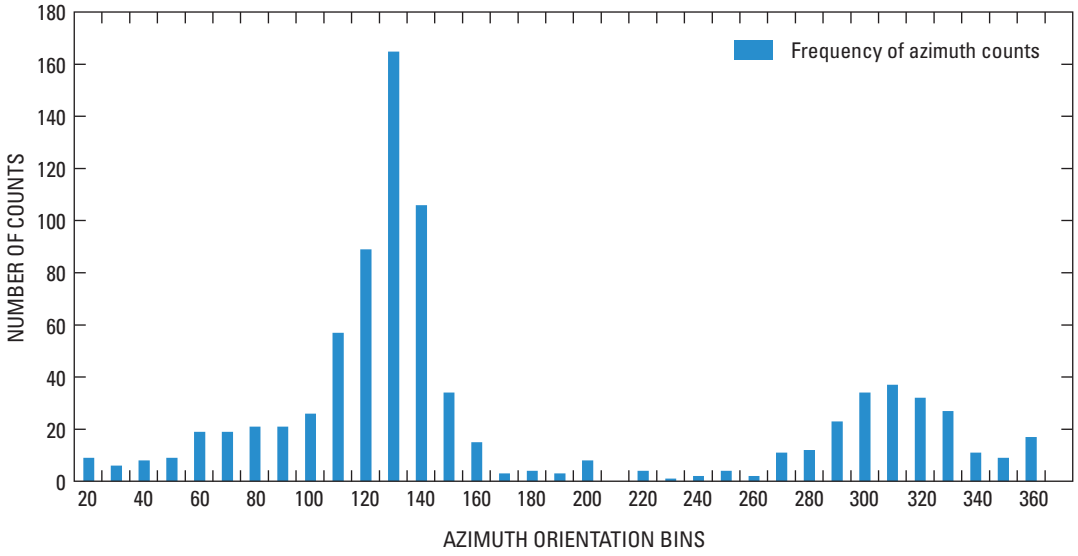

Appendix 2. Borehole foliation dip azimuth frequency distribution graphs as determined from optical televiewer images in well Oaks-2.

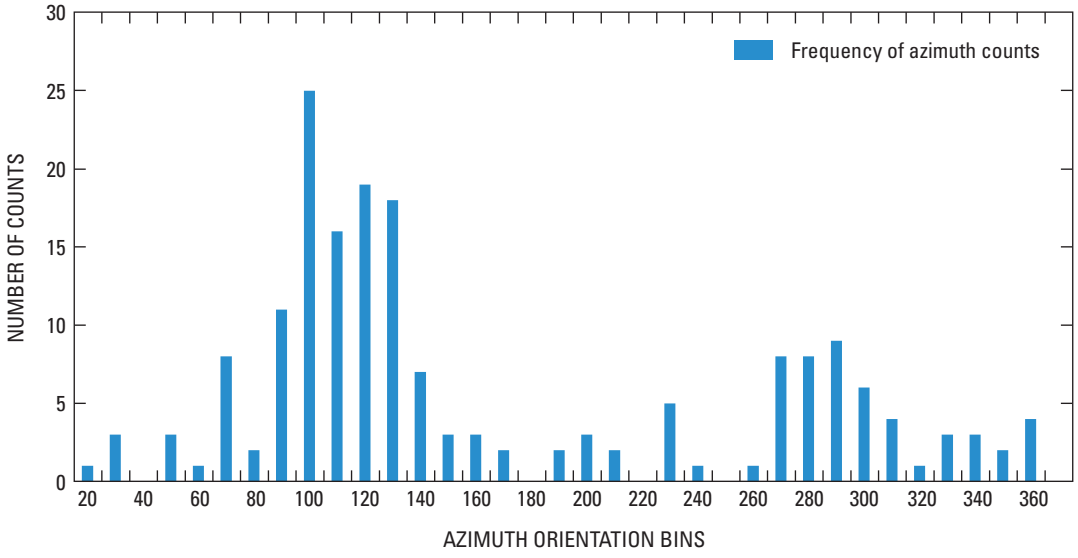

Appendix 2. Borehole foliation dip azimuth frequency distribution graphs as determined from optical televiewer images in well ERT-6.

Appendix 3

Orientations of borehole fractures within packer zones from the following wells and depth intervals:

Well 1: 68–78, 252–262, and 288–298 ft bls

Well CHR: 40–78, 80–90, and 484–504 ft bls

Well AW-4: 115–121 and 680–690 ft bls

Well AW-5: 0–101, 183–189, 200–210, 418–428, and 560–570 ft bls

Well AW-7: 53–58, 88–94, 167–173, 229–239, and 450–460 ft bls

Well ERT-7: 6–13, 60–67, 69–75, and 80–86 ft bls

Well Oaks-2: 20–50, 64–70, 153–170, 580–590 ft bls

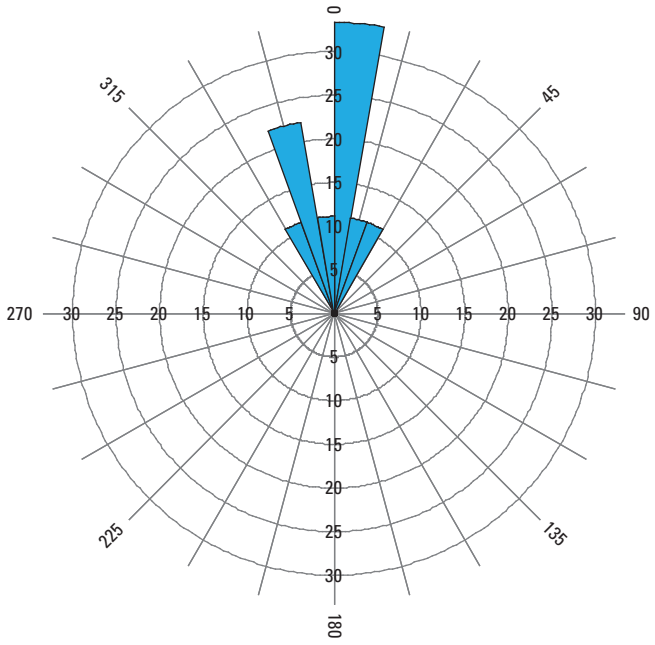

WELL DEPTH, 68–78 FEET BELOW LAND SURFACE

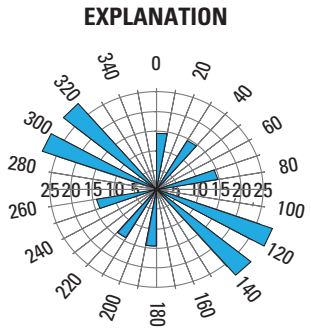

Rose diagram displaying strike azimuth of measured borehole fractures. Length of petal corresponds to percentage of measurements.

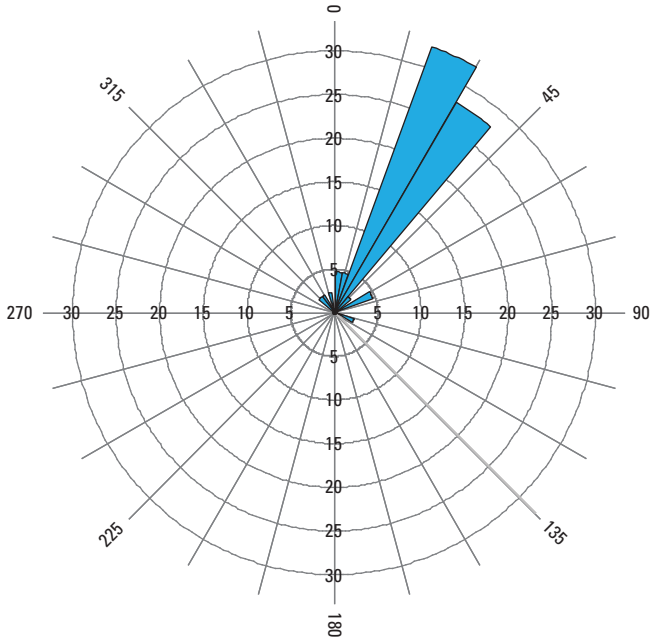

WELL DEPTH, 252–262 FEET BELOW LAND SURFACE

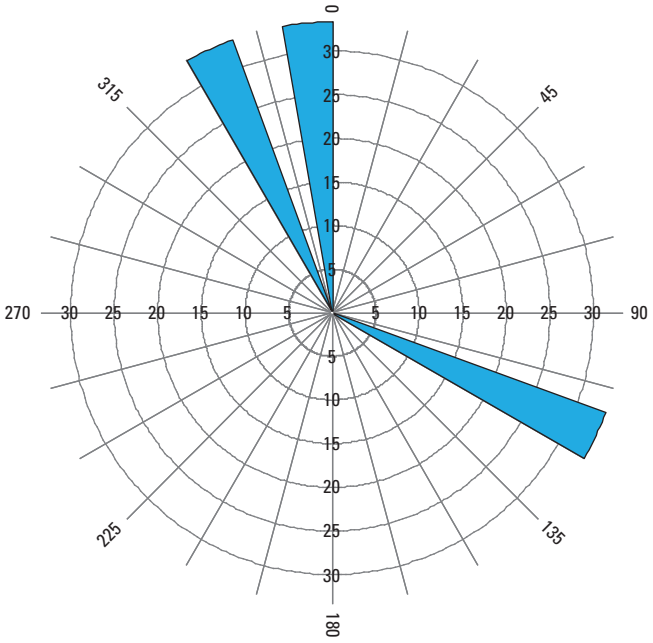

WELL DEPTH, 288–298 FEET BELOW LAND SURFACE

Appendix 3. Orientations of borehole fractures within packer zones from Well 1 at indicated depth intervals.

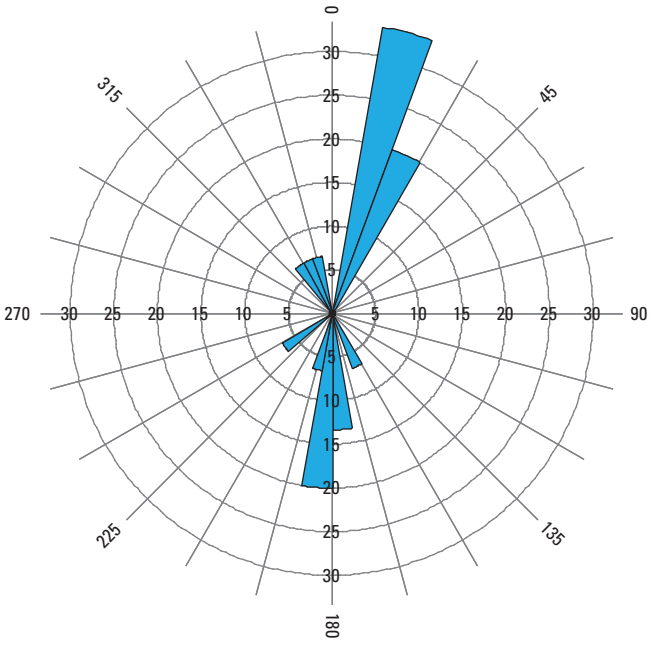

WELL DEPTH, 40–78 FEET BELOW LAND SURFACE

EXPLANATION

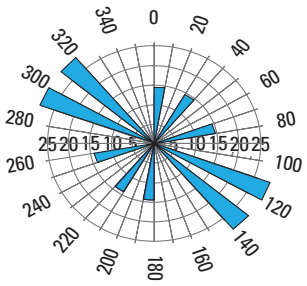

Rose diagram displaying strike azimuth of measured borehole fractures. Length of petal corresponds to percentage of measurements.

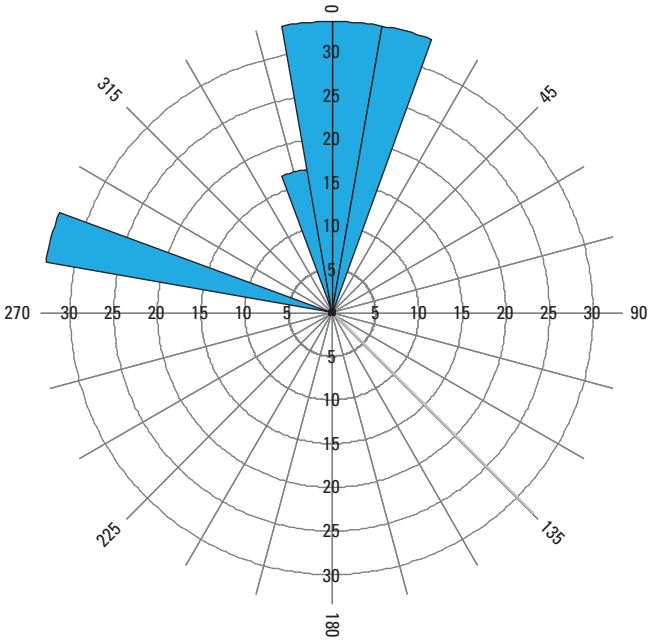

WELL DEPTH, 80–90 FEET BELOW LAND SURFACE

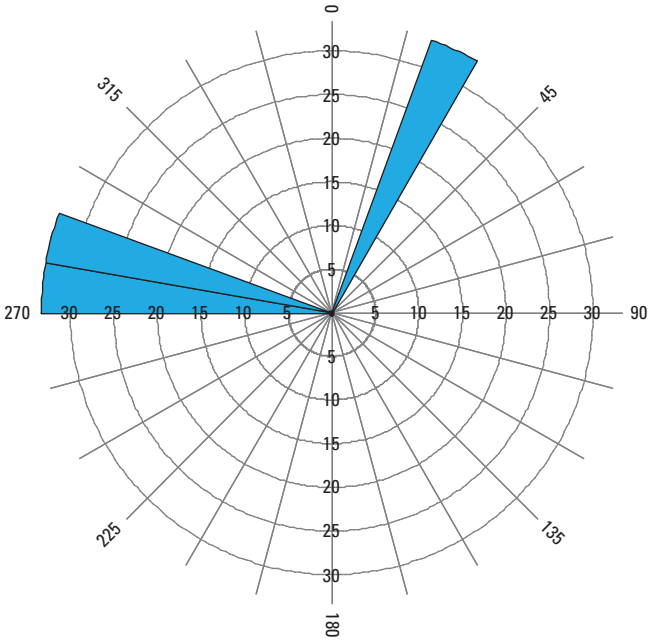

WELL DEPTH, 484–504 FEET BELOW LAND SURFACE

Appendix 3. Orientations of borehole fractures within packer zones from well CHR at indicated depth intervals.

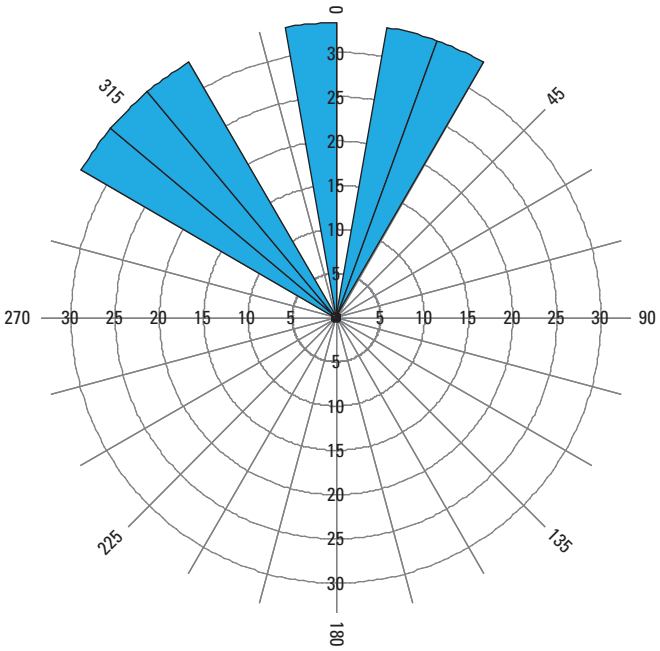

WELL DEPTH, 115–121 FEET BELOW LAND SURFACE

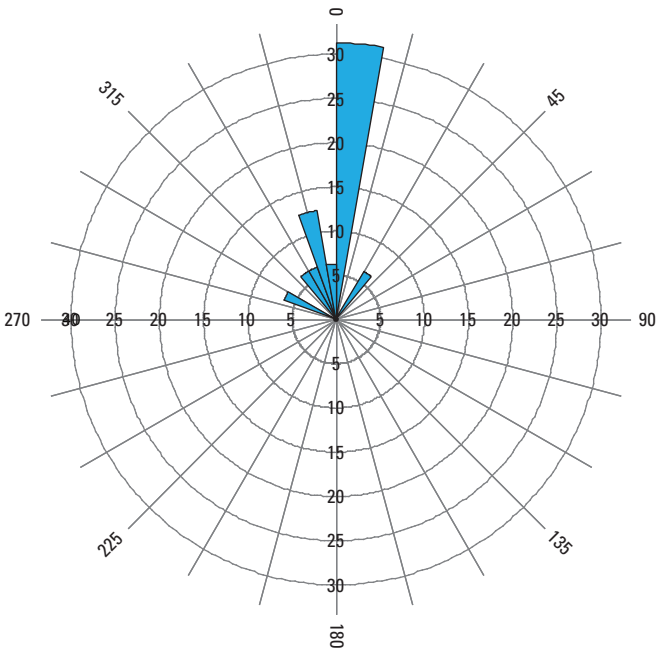

WELL DEPTH, 680–690 FEET BELOW LAND SURFACE

EXPLANATION

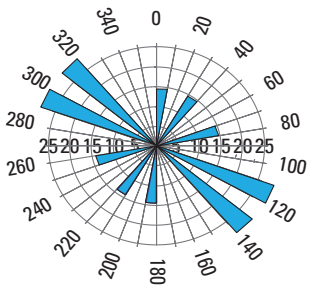

Rose diagram displaying strike azimuth of measured borehole fractures. Length of petal corresponds to percentage of measurements.

Appendix 3. Orientations of borehole fractures within packer zones from well AW-4 at indicated depth intervals.

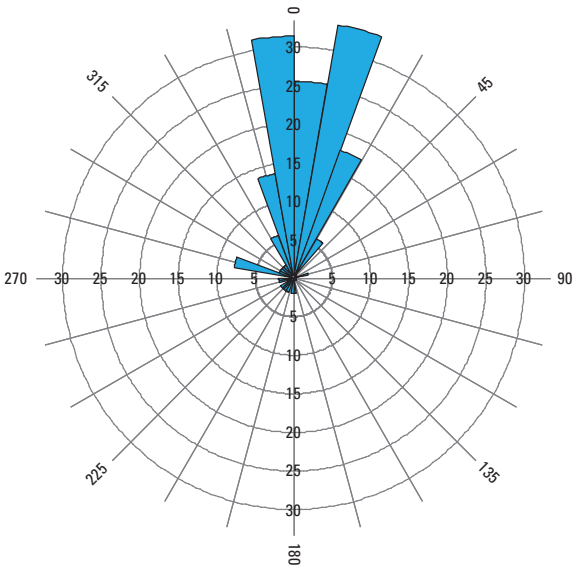

WELL DEPTH, 0–101 FEET BELOW LAND SURFACE

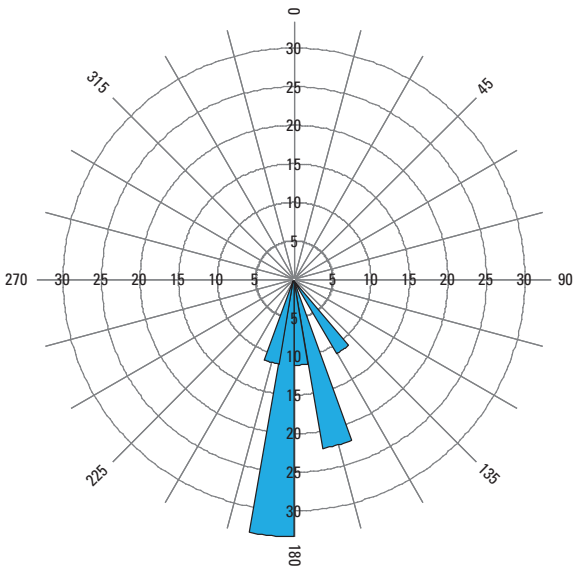

WELL DEPTH, 183–189 FEET BELOW LAND SURFACE

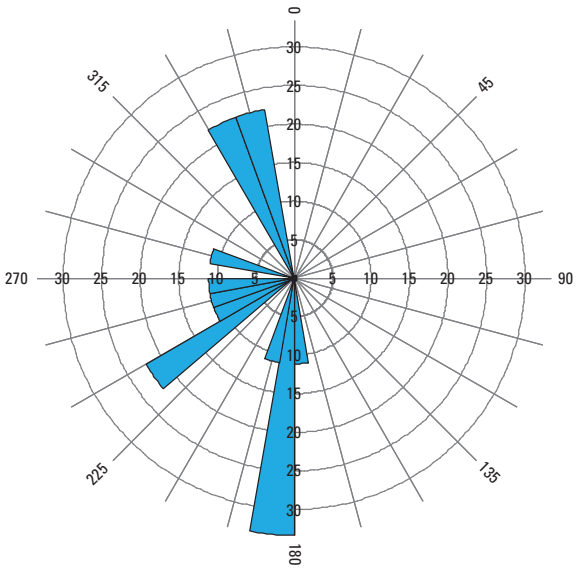

WELL DEPTH, 200–210 FEET BELOW LAND SURFACE

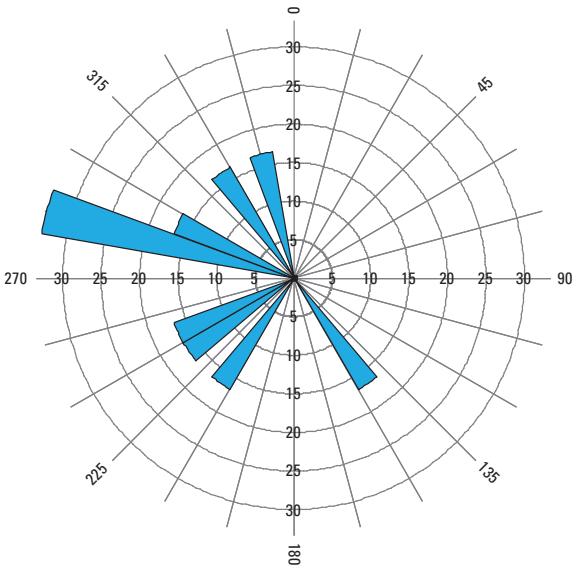

WELL DEPTH, 418–428 FEET BELOW LAND SURFACE

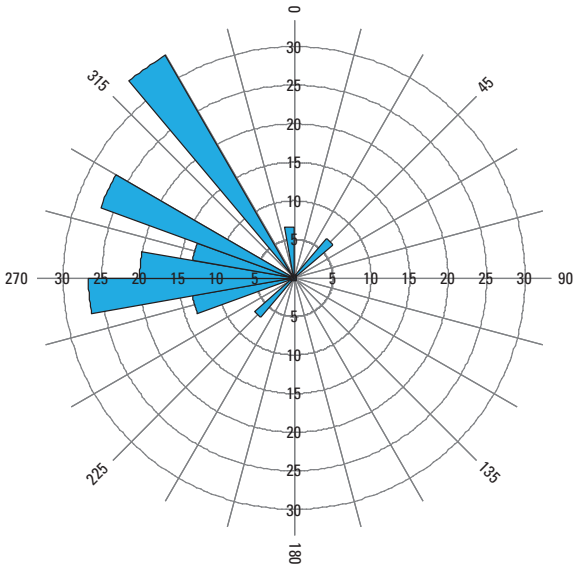

WELL DEPTH, 560–570 FEET BELOW LAND SURFACE

EXPLANATION

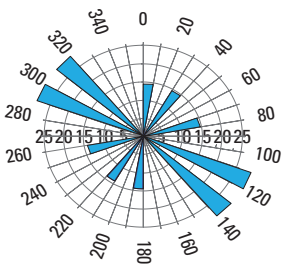

Rose diagram displaying strike azimuth of measured borehole fractures. Length of petal corresponds to percentage of measurements.

Appendix 3. Orientations of borehole fractures within packer zones from well AW-5 at indicated depth intervals.

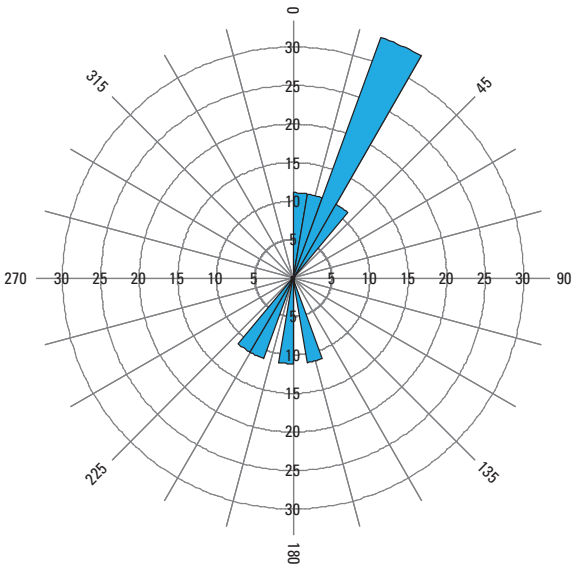

WELL DEPTH, 53–58 FEET BELOW LAND SURFACE

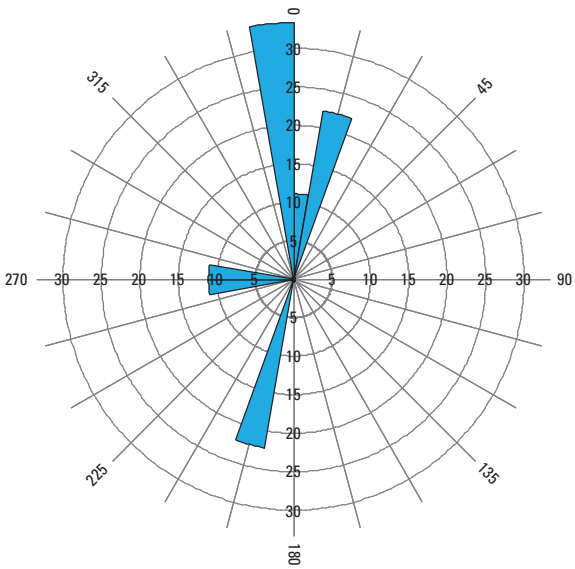

WELL DEPTH, 88–94 FEET BELOW LAND SURFACE

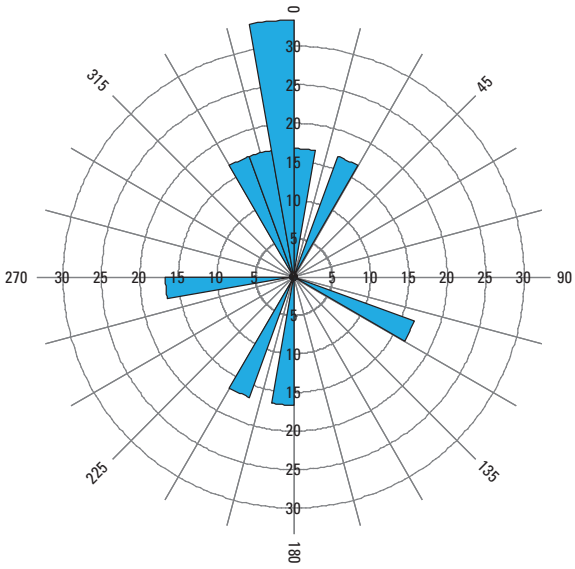

WELL DEPTH, 167–173 FEET BELOW LAND SURFACE

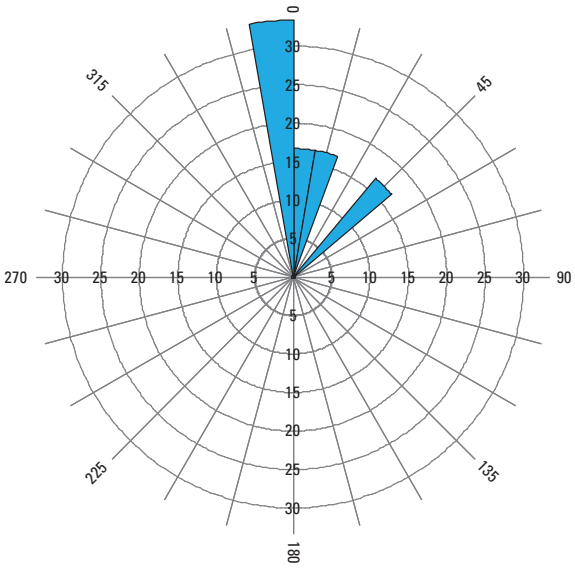

WELL DEPTH, 229–239 FEET BELOW LAND SURFACE

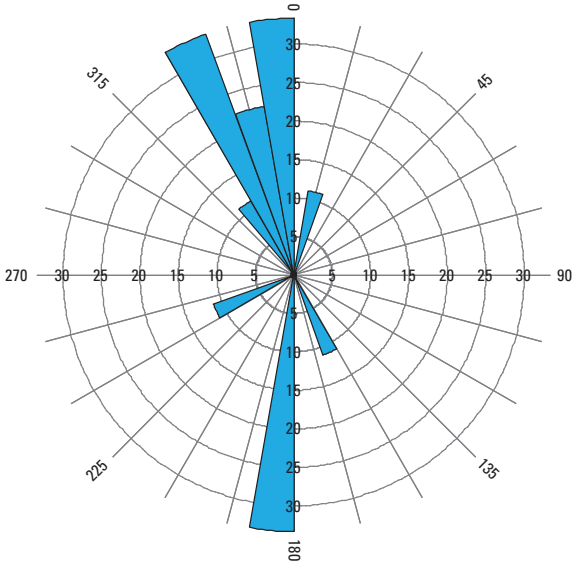

WELL DEPTH, 450–460 FEET BELOW LAND SURFACE

EXPLANATION

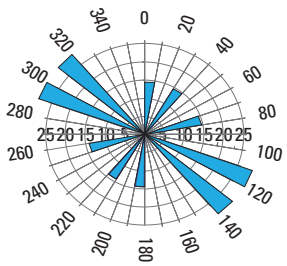

Rose diagram displaying strike azimuth of measured borehole fractures. Length of petal corresponds to percentage of measurements.

Appendix 3. Orientations of borehole fractures within packer zones from well AW-7 at indicated depth intervals.

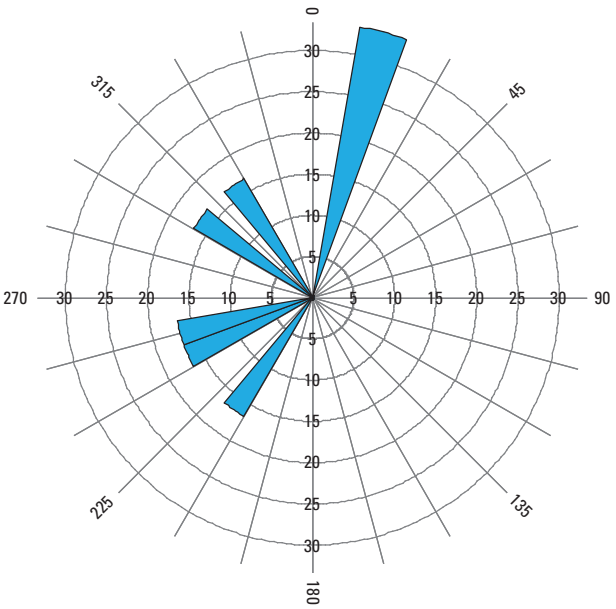

WELL DEPTH, 6–13 FEET BELOW LAND SURFACE

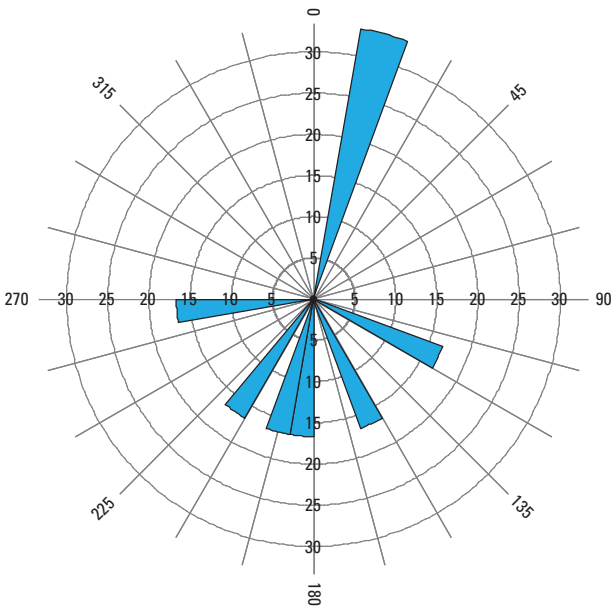

WELL DEPTH, 60–67 FEET BELOW LAND SURFACE

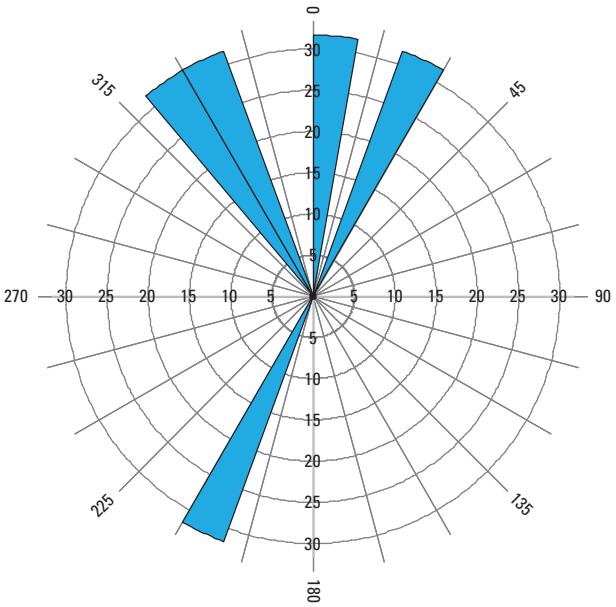

WELL DEPTH, 69–75 FEET BELOW LAND SURFACE

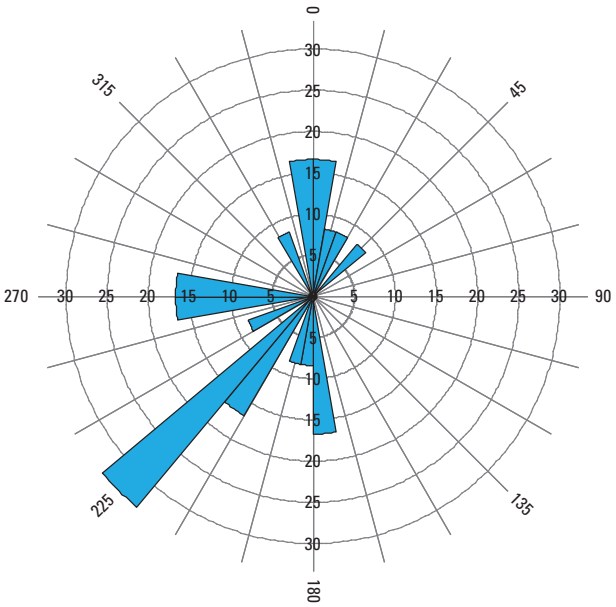

WELL DEPTH, 80–86 FEET BELOW LAND SURFACE

EXPLANATION

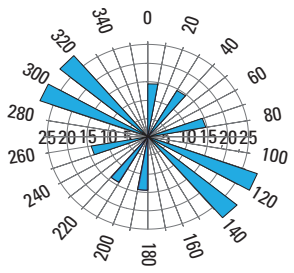

Rose diagram displaying strike azimuth of measured borehole fractures. Length of petal corresponds to percentage of measurements.

Appendix 3. Orientations of borehole fractures within packer zones from well ERT-7 at indicated depth intervals.

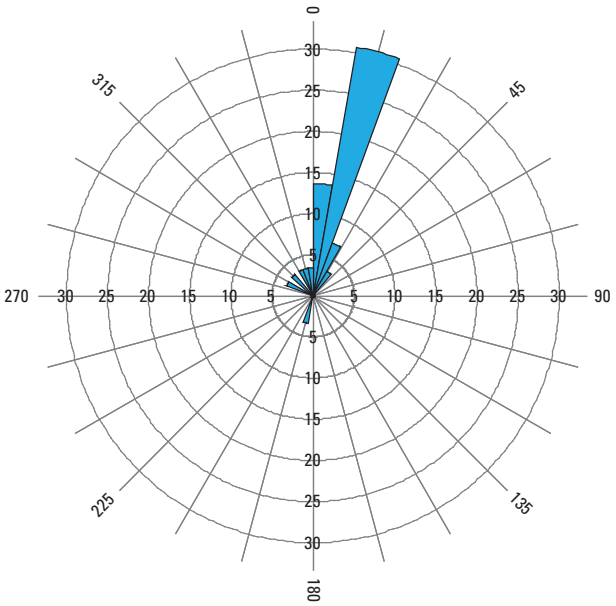

WELL DEPTH, 20–50 FEET BELOW LAND SURFACE

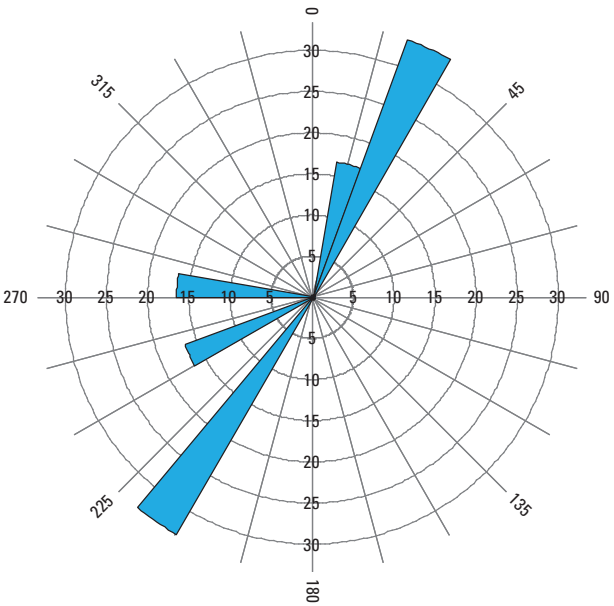

WELL DEPTH, 64–70 FEET BELOW LAND SURFACE

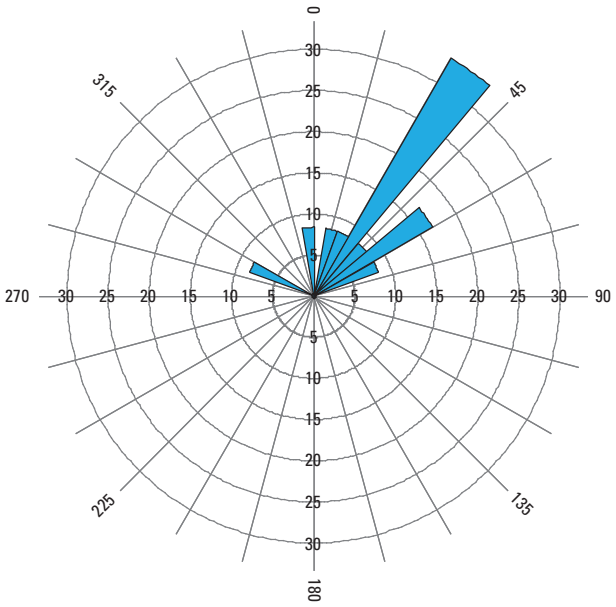

WELL DEPTH, 153–160 FEET BELOW LAND SURFACE

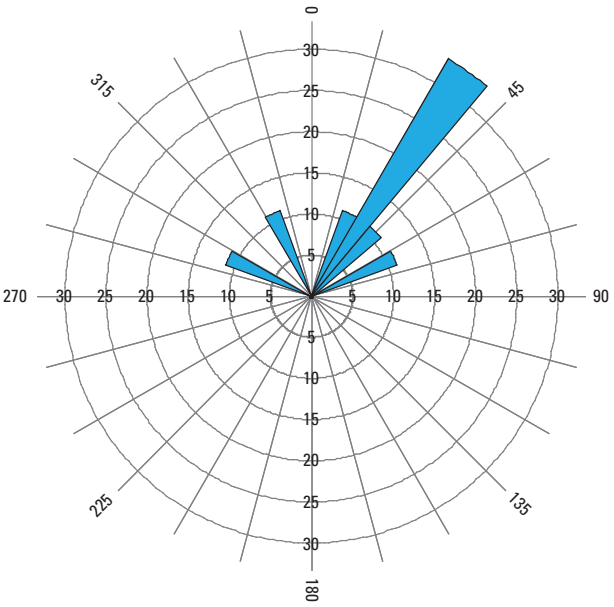

WELL DEPTH, 580–590 FEET BELOW LAND SURFACE

EXPLANATION

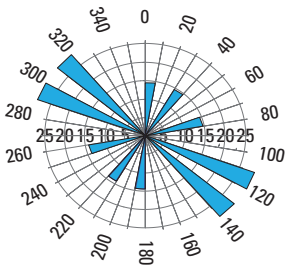

Rose diagram displaying strike azimuth of measured borehole fractures. Length of petal corresponds to percentage of measurements.

Appendix 3. Orientations of borehole fractures within packer zones from well Oaks-2 at indicated depth intervals.

Prepared by:
U.S. Geological Survey
Enterprise Publishing Network
Raleigh Publishing Service Center
3916 Sunset Ridge Road
Raleigh, NC 27607

A PDF version of this publication is available online at
http://pubs.usgs.gov/ds/538/